JAERI-Tech
2001-044

ANALYTICAL STUDY OF NARROW CHANNEL FLOW FOR A SPALLATION TARGET SYSTEM DESIGN

July 2001

Md. Shafiqul Islam*, Atsuhiko TERADA, Hidetaka KINOSHITA,
Ryutaro HINO and Masanori MONDE*

日本原子力研究所
Japan Atomic Energy Research Institute

本レポートは、日本原子力研究所が不定期に公刊している研究報告書です。
入手の問合わせは、日本原子力研究所研究情報部研究情報課（〒319-1195　茨城県那珂郡東海村）あて、お申し越しください。なお、このほかに財団法人原子力弘済会資料センター（〒319-1195　茨城県那珂郡東海村日本原子力研究所内）で複写による実費頒布をおこなっております。

This report is issued irregularly.
Inquiries about availability of the reports should be addressed to Research Information Division, Department of Intellectual Resources, Japan Atomic Energy Research Institute, Tokai-mura, Naka-gun, Ibaraki-ken 319-1195, Japan.

編集兼発行　日本原子力研究所

Analytical Study of Narrow Channel Flow for a Spallation Target System Design

Md. Shafiqul Islam*, Atsuhiko TERADA※, Hidetaka KINOSHITA,
Ryutaro HINO and Masanori MONDE*

Center for Neutron Science
Tokai Research Establishment
Japan Atomic Energy Research Institute
Tokai-mura, Naka-gun, Ibaraki-ken

(Received May 8, 2001)

Heat transfer and pressure drop characteristics under fully developed turbulent water flow condition were analyzed over a two-dimensional narrow rectangular channel whose height is H=1.2 mm. The channel configuration and water flow condition simulate forced convection cooling of a spallation target system components design such as a solid target and a proton beam window. The high-Reynolds number form of the standard $k-\varepsilon$ and RNG$k-\varepsilon$ models employing wall functions for the Reynolds number (Re) range of 7,000 to 22,000 were used in the analyses. As for heat transfer characteristics of a smooth channel, the Nusselt number obtained by the standard $k-\varepsilon$ model agreed very well with the Dittus-Boelter correlation. No significant differences in friction factors for the smooth channel were observed for these two models, which agreed well with the Blasius correlation. However, the standard $k-\varepsilon$ model could not predict friction factors well for the rib-roughened channel.

Keywords: Pressure Drop, Turbulent Flow Heat Transfer, Narrow Channel, Two-dimensional Analysis, Forced Convection, Spallation Target System, Turbulent Model, Wall Functions.

※ On leave from Ishikawajima-Harima Heavy Industries Co., Ltd.

* Saga University

核破砕ターゲットシステム設計のための狭い流路における流れの解析的研究

日本原子力研究所東海研究所中性子科学研究センター

Md. Shafiqul Islam*・寺田　敦彦※・木下　秀孝・日野　竜太郎・門出　政則*

（２００１年５月８日　受理）

高さ 1.2mm の 2 次元狭隘矩形流における十分に発達した乱流域での水の熱伝達と圧力損失特性を水流動条件で解析した。流路形状や流動条件は核破砕ターゲットシステムにおける陽子ビーム窓や固体ターゲット模擬した。解析は高レイノルズ数モデルの標準 $k-\varepsilon$ モデルと RNG $k-\varepsilon$ モデルを用い、壁関数を利用してレイノルズ数(Re) が 7,000～22,000 の範囲で行った。平滑流路における熱伝達特性に関しては標準 $k-\varepsilon$ モデルで得られたヌセルト数は Dittus-Boelter の式とよく一致した。二つの乱流モデルで計算される摩擦損失係数に大きな違いはなく、ブラジウスの式とよく一致した。なお、リブ付き流路の摩擦損失係数に関しては 良い予測は得られなかった。

東海研究所：〒319-1195　茨城県那珂郡東海村白方白根 2-4

※外来研究員：石川島播磨重工業㈱

＊ 佐賀大学

Contents

目 次

1. Introduction

The Japan Atomic Energy Research Institute (JAERI) and the High Energy Accelerator Research Organization (KEK) are jointly developing a next generation neutron source using a high-intensity proton accelerator in order to use high-intensity neutrons in the fundamental sciences and nuclear engineering fields. The proposed spallation neutron source will use a proton beam power up to as high as 5 MW. Development of a MW-class spallation neutron source is one of the most difficult technical challenges. Two types of targets, namely, a mercury target and a solid target which work as spallation neutron sources have been proposed [1]. According to the conceptual spallation mercury target system design [2], it consists of a target vessel and a safety hull. A 1 MW pulsed proton beam from the high-intensity proton accelerator will be injected into the mercury target to produce high-intensity neutrons. With the spallation reaction of the injected proton beam and mercury nucleus, huge amount of heat will be generated and deposited in mercury. For the safety design of the MW-class mercury target system, sufficient heat removal with a slow mercury flow is necessary to prevent corrosion and erosion of the target vessel. According to the conceptual solid target system design [1], the solid target consists of heavy metal target plates made of tungsten, and it could be used under a proton beam power up to 2.5 MW. Through the spallation reaction between the pulsed proton beam with 1 μs pulse length up to 50 Hz and the tungsten nucleus, huge amount of heat will be generated and deposited in the target plates. Thus, it is necessary to remove this huge amount of heat generation efficiently in order to maintain structural integrity.

Another important technical aspect in the spallation neutron source facility is to design the proton beam window [3], which acts as a boundary between a proton beam line (vacuum) and the target system (helium atmosphere). The proton beam window consists of two Inconel plates and located at the end of the proton beam line. There will be a high heat deposition in these plates, and it is necessary to cool down the plates so as to avoid excessive thermal stress. Cooling channels in the solid spallation target and the proton beam window are very narrow in order to minimize water volume, which affects the neutron yield. In order to remove huge amount of heat generation from the spallation target system components, heat transfer enhancement technique using repeated-micro-ribs working as turbulent promoters in a narrow water-flow channel has been proposed. Smooth narrow channel will cause not only high coolant velocity but also flow-induced vibration, erosion and flow disruption. A brief description of spallation

target system components are described in **Chap. 2**. The main objective in this study is to make clear heat transfer and pressure drop characteristics under turbulent flow condition in a narrow channel for a spallation target system components design by numerical analyses.

2. High Heat Flux Components in a Spallation Target System

In the conceptual spallation mercury target system design, an integrated structure of target vessel with the safety hull was proposed to ensure the safety and to collect mercury in case of mercury leakage caused by the target beam window failure. The inner structure arrangement of the mercury target vessel was determined based on thermal-hydraulic analytical results of 3 GeV, 1 MW proton beam injection. The mercury target currently under conceptual design adopted a cross-flow type (CFT) target vessel. **Figure 1** shows the cutaway view of CFT mercury target with the safety hull. Mercury enters into the target from the furthest side from the beam window and flows along the blade flow distributor in the inlet plenum toward each end of the blade, and then crosses over the proton beam and returns through the outlet plenum along the blades. The target vessel will be made of 316-stainless steel and its size presently under design is 260 mm in width, 80 mm in height in front of the target and 800 mm in effective length. In order to ensure safety of the target system, the integrated structure of target vessel with the safety hull was proposed as shown in **Fig. 2**. The vessels for mercury target, helium and heavy water will be connected each other by reinforcement ribs mounted on the surface of each vessel by welding. The safety hull consists of helium and heavy water vessels, which is known as outer vessel. Narrow heavy water-flow channel by introducing repeated-micro-ribs inside will be used to remove excessive heat of outer vessel's beam window.

In the conceptual spallation solid target system design, the solid target consists of tungsten target plates and it could be used against a proton beam power up to 2.5 MW. There will be 39 target plates of which thickness varied from 6~25 mm with dimensions of 170 mm in length and 70 mm in height. They will be arranged in a row against injected high-intensity proton beam power up to 2.5 MW. **Figure 3** shows the concept of the solid target. Heavy water will be used as a coolant to minimize the neutron capture and it flows horizontally to cool down the target plates. Heavy water will also be used to cool down the outer vessel of the target container under the 2.5 MW proton beam operation. **Figure 4** shows the power density calculation result of the solid targets assuming uniform proton beam profile. According to Fig. 4, the maximum heat flux is

calculated to be 1.28 MW/m^2 under 2.5 MW operation. Through the spallation reaction between the proton beam and the target nucleus, high-density heat up to 1.2 kW/cm^3 will be generated in the target plates. The maximum heat flux reaches 3.6 MW/m^2 even in thin target plate, which has a thickness of 6 mm. The cooling channels between the plates are very narrow in order to decrease water volume ratio affecting the neutron yield. In the current solid target design, the gap of water-flow channel is 1.2 mm and water volume ratio to the target metal volume is being kept to less than 10 %. Repeated-micro-ribs on one side of the target plates are adopted in order to remove this high heat flux efficiently.

Another important aspect of high heat flux component of a spallation target system is the proton beam window that locates at the end of proton beam line and acts as a pressure boundary between vacuum and helium atmosphere. It consists of two Inconel plates, which are cooled down by heavy water flowing vertically from the bottom to the top of the plates. In the current proton beam window design, the gap of a water-flow channel is 5 mm. **Figure 5** shows the concept of a flat-type proton beam window to be applied to a 5 MW proton beam operation. The dimension of a proton beam window is 330 mm in width, 235 mm in height and 65 mm in depth. Light water flowing from two inlet pipes is adjusted by using flow guides in order to distribute its flow rate uniformly in the window section. The maximum volumetric heat deposition at the window will be 960 W/cm^3 under 5 MW operation. The thickness of the window will be less than 3 mm. Repeated-micro-ribs will also be formed on one side of the plates.

To design the cooling channel between the target plates and the proton beam window, heat transfer enhancement using repeated-micro- ribs working as turbulent promoters in a narrow channel has been proposed so as to remove high heat flux to keep the temperature of the target plates and mercury target vessel sufficiently low with relatively low coolant velocity. It is difficult to comprehend the heat transfer mechanism in the turbulent flow regime due to eddy, separation, and reattachment. Even though these difficulties, it is necessary to make clear the heat transfer and pressure loss characteristics in a rib-roughened narrow channel both analytically and experimentally in order to understand the mechanism of heat transfer enhancement better and to design the target system components.

Many studies on heat transfer enhancement using repeated ribs have been carried out both analytically and experimentally on tubes and annuli under air-flow conditions but very few studies are on narrow rectangular channels under water-flow condition. There are virtually almost no heat transfer data available both analytically and experimentally

on a very narrow rectangular channel with repeated-micro-ribs under water-flow condition. Islam et al. [4] investigated for the first time to measure the heat transfer and pressure loss data experimentally [4] on such a narrow rectangular channel with repeated-micro-ribs under water-flow condition. The data revealed that a high potential heat transfer in the rib-roughened narrow channel but fluid flow and heat transfer mechanisms are not yet made clear. In this study, in order to understand the complex mechanism numerically, a CFD analytical tool, the Star-CD code, was selected. Engineering practice is also necessary to use empirical roughness functions to describe the near wall region, and analytical or numerical solution scheme to calculate the core flow in the narrow smooth and rib-roughened channel.

The $k-\varepsilon$ model is presently the most widely used turbulent model for practical analyses and has been built into virtually all-commercial general-purpose CFD codes. Bridging the viscosity-affected near-wall layers with the wall functions, most calculations carry out so far with the $k-\varepsilon$ model. The wall functions involving the friction velocity are of course particularly unsuited for separation and reattachment regions where the friction velocity changes significantly. In order to make the $k-\varepsilon$ model applicable to the viscosity-affected near-wall region, the standard high-Re–number version had to be modified by replacing some of its constants by viscosity-dependent functions and additional terms in the $k-\varepsilon$ equations. This is the "low-Re-number and two-layer models" approach that had been used for simulating the turbulent processes very near walls.

The cross-sectional geometries of a flow channel with and without repeated-micro-ribs surfaces of this study are shown in **Figs. 6** and **7,** respectively. Their dimensions are also figured out. Each of channels consists of a space enclosed by solid walls with an inlet and an outlet. The fluid within the geometry is water and its thermo-physical properties are evaluated at 15℃. The total mass entering the channel exits through the outlet. The flow is assumed to be two-dimensional turbulent flow with constant fluid temperature, density and viscosity. The high-Re-number form of the standard $k-\varepsilon$ and RNG $k-\varepsilon$ turbulent models were used in the analyses. The analyses were performed for the non-heating and heating with uniform wall heat flux from one-side, for a range of the Reynolds numbers from 7,000 to 22,000. The various investigations carried out on rib-roughened surfaces both experimentally and analytically to date have been presented in **Chap. 3.**

3. Literature survey

Improvements of heat transfer performance through passive and active enhancement methods have been studied intensively for over 30 years. Heat exchangers with single-phase tube-side flow are one of the important applications where passive surface-modification methods are popularly applied. Typical examples of passive heat transfer enhancement techniques are:

(i) Surface roughness
(ii) Displaced turbulent promoters, and
(iii) Swirl flow generators.

Surface roughness is one of the promising techniques to be considered seriously as a means of enhancing forced-convection with single-phase flow heat transfer. Initially it was speculated that elevated heat transfer coefficients might accompany the relatively high friction factors of rough conduits. However, since the commercial roughness is not well defined, artificial surface roughness-introduced through knurling or threading or formed by repeated-rib turbulent promoters has been employed. Although the enhanced heat transfer with turbulent promoters is often due to the fin effect, it is difficult to separate the fin contribution. In certain cases it may be desirable to leave the heat transfer surface intact and achieve the enhancement by disturbing the flow near the heated surface. Displaced turbulent promoters alter flow mechanics near the surface by disturbing the core flow and can be done by placing thin rings or discs in a tube. It is seen that the rings substantially improve heat transfer in the lower Reynolds number range where the discs are not particularly effective. Examples are baffles and mixing elements. It has been established that the swirling flow will improve heat transfer in a duct flow. Generating of swirl flow has been accomplished by coil wires, spiral fins, stationary propellers, coiled tubes, inlet vortex generators, and twisted tapes. All of these heat transfer enhancement methods improve single-phase and boiling heat transfer at the expense of increased pumping power. Heat transfer coefficients are relatively high for vortex flow due to an increase in velocity and a secondary flow produced by the radial body force when a favorable density gradient is present and a fin effect with certain continuous swirl generators.

With the passage of time, the above types of surface roughness are being utilized more and more for enhancement of heat transfer. Active enhancement, which has also been studied extensively, requires the additional of external power to achieve the desired flow modification. They include heat transfer surface vibration, fluid vibration, and

electrostatic field introduction, are costly and complex. Of the several methods discussed above, the most popular and successful technique is the enhancement through surface roughness. This is mainly because of its effectiveness in enhancing the heat transfer, relatively easy to manufacture, less cost and simplicity in application. Ribs, indentations, spiral flutes and coil inserts are some common surface modification (roughness) techniques that are currently used or have been proposed for single-phase heat transfer applications. Of these, two-dimensional transverse type repeated-rib promoter is unique because of the two-dimensional flow field and the design control parameters are just the rib height (k), rib spacing (p) and the rib shape. As for spirally indented, fluted and ribbed tubes, the flow field becomes three-dimensional where a helix angle becomes an additional and essential design parameter.

Such rib-roughened tubes are sometimes considered in the design of shell-and-tube heat exchangers. For examples, they applied include single-phase tube of flooded chillers for air conditioners, surface of condensers for power plants. The size of these heat exchangers can be reduced considerably by use of rib-roughened tubes instead of smooth tubes. This has important potential applications of large systems such as those used in thermal, geothermal, and ocean thermal energy conversion (OTEC) power plants, which require very large heat exchangers. In addition to these applications, narrow channel with repeated-rib type promoters is now considered to be applied for the high heat flux spallation target components. In spite of increasing the use of these rib-roughened tubes or channels, there are no general correlations available for quantitative evaluation of pressure drop and heat transfer. In one of the early studies on ribbed tubes, Kalinin et al. [5] proposed correlations for pressure drop and heat transfer. However, the correlations are valid only for transverse ribs within the specific ranges of k/D_e=0.016-to-0.07 and p/D_e=0.25-to-1.0, respectively.

Many of the studies found in the literature have tried to extend the studies of Nikuradse [6] on friction with sand-grain roughness and the heat transfer-momentum-transfer analogy of Dipprey and Sabersky [7] for this type of roughness, while Gee and Webb [8] proposed correlations for helical ribs, without including the effects of the pitch. The most general correlations to date were proposed by Withers [9], Li et al.[10], and Nakayama et al.[11] for helically ribbed tubes. Han et al. [12] systematically investigated the effects of the rib pitch-to-height ratio (p/k), the height-to-equivalent diameter ratio (k/D_e) and the effect of helix angle (α_a) on the heat transfer coefficient and the friction factor of fully developed turbulent air flow in ducts

that had two or four opposite rib-roughened walls. Liou et al.[13] also presented the simplest correlations to see the effects of rib shapes on turbulent heat transfer and friction in a rectangular channel. The Webb et al.[14] correlations are applicable to water, air and n-butyle alcohol for transverse repeated-rib roughness in a tube.

A comprehensive list was prepared consisting of all the experimental investigations from which heat transfer and friction factor data could be extracted for different roughened surfaces for single-phase turbulent flow in internally roughened tubes up to now. No restrictions were placed on the flow parameters, namely, the Reynolds number and the Prandtl number, even though much of the data were obtained in the turbulent regime with either air or water as the test fluid. This file lists the authors of the investigation and the type of enhanced tubes along with number of tubes tested in the experiments, which are summarized in **Table 1**. The sources are listed in the reference section. In addition, the type of experiment, whether the fluid is heated or cooled, and the method of heat transfer are provided whenever possible for future reference.

In addition to numerous experimental studies cited above, a number of numerical studies have also been performed in order to predict the flow behavior in near-wall region and flows past two-dimensional ribs. Typical numerical studies with the linear $k-\varepsilon$ model (Launder and Spalding, [43]) are: Lewis [44], Lee et al.[45], Patankar et al.[46] Liou et al.[47], Durst and Rastogi [48], Yap [49], Jones and Launder [50], Benodekar et al.[52], Chung et al.[53], Park and Chung [54], and Leschziner and Rodi[51].

The first attempt to analytical determination of the roughness functions for flow over rectangular ribs was made by Lewis [44]. The flow was approximated by a series of attached and separated flow regions, and some empirical information from experiments over cavities and steps was required. The $k-\varepsilon$ turbulent model with wall function boundary conditions was used by Lee et al.[45] to predict roughness functions in an annulus with a ring type rectangular roughness on the inner pipe. In a numerical study, a fully developed flow in a single module was solved using the periodicity conditions, as proposed by Patankar et al. [46] in order to avoid the entrance region effect. Liou et al. [47] made numerical computations for turbulent flow over a single rib-roughness in a channel. Numerical calculations for flow over two-rib roughness in a channel were performed by Durst et al. [48].

Recently Yap [49] has made a numerical study using various turbulent models. The best heat transfer prediction was obtained with a low-Re-number $k-\varepsilon$ turbulent model

across the viscous sublayer and an algebraic stress model in the core flow. However, the Jones and Launder version [50] of the low-Re-number $k-\varepsilon$ model employed for the whole flow regime gave fairly good predictions, provided an appropriate source term was added to the transport equation for the turbulent dissipation rate. Yap[49] also found that the wall function approach showed poor Reynolds number dependence for the peak Nusselt Number, even with the algebraic stress model employed in core. Leschziner and Rodi [51] derived the standard $k-\varepsilon$ turbulent model with and without the curvature correction equation to solve for the turbulent flow field and heat transfer between successive ribs in the periodic fully developed regime of a ribbed annulus. Applying this correction of the $k-\varepsilon$ model to the analyses of annular and twin parallel jets, they obtained greatly improved predictions compared with the standard $k-\varepsilon$ model.

Durst and Rastogi [48], Benodekar et al. [52], Chung et al. [53], and Park and Chung [54] have also carried out comparisons between $k-\varepsilon$ model results with and without curvature corrections, and experimental results. Standard wall functions were used in all these numerical studies. Use of wall functions as boundary conditions when solving turbulent flows using the $k-\varepsilon$ model has been relatively successful where properties are constant. But for large and irregular property variations in the viscous sublayer and buffer layers, the use of wall functions presents a fundamental problem. Large and irregular property variations of water at high temperature would complicate the development of reference property schemes as a reference property scheme can be used in the wall functions. Since many investigations have been carried out both experimentally and analytically on tubes and annuli under air-flow conditions but very few studies are on narrow rectangular water-flow channel. There are almost no heat transfer data available both experimental and analytical on a very narrow rectangular channel with one-side repeated-ribs and one-side constant heat flux under water-flow condition. The objective of this literature survey is to make clear that thermal-hydraulic studies by experimentally and analytically on such a narrow channel would be the first step to date.

4. Turbulent model performance in narrow channel flows

4.1 Description of problems

Problems to be considered in this study are depicted schematically in **Figs. 8** and **9,** respectively. Each of them involves the determination of two-dimensional heat transfer and fluid flow characteristics for turbulent forced-convection cooling. The computational

geometry of smooth and rib-roughened narrow rectangular channels consist of a space enclosed by solid walls with an inlet and an outlet and its major controlling parameters are shown below. A uniform heat flux is supplied from the bottom side and the opposite side is insulated so as to remain adiabatic condition. The fluid within the geometry is water and its thermo-physical properties at 15℃ are as follows:

(i) Density, ρ = 997.09 kg /m^3
(ii) Molecular viscosity, μ = 890.72 × 10^{-6} Pa s
(iii) Specific heat, C_p = 4180.0 J / (kg K)
(iv) Thermal conductivity, λ = 0.604 W/(m K)
(v) Molecular Prandtl number, Pr = 8.06

The total mass entering the geometry exits through the outlet. The flow is assumed to be two-dimensional turbulent one with constant fluid temperature, density and viscosity.

(1) Modeling Strategy

The following modeling strategy is used:

(i) Cartesian coordinate system with uniformly spaced hexahedral cells
(ii) Inlet, outlet, wall and symmetry plane boundary conditions.
(iii) Incompressible and steady flow options.
(iv) Appropriate physical parameters for water
(v) $k-\varepsilon$ turbulent models for the turbulent characteristics

(2) Analytical Procedure

In each model, the channel height (H) was fixed for 1.2 mm, an entrance and an exit lengths for 0 - 25 mm and a heating length for 200 mm as a reference that was assumed in the conceptual design of the solid target [1].

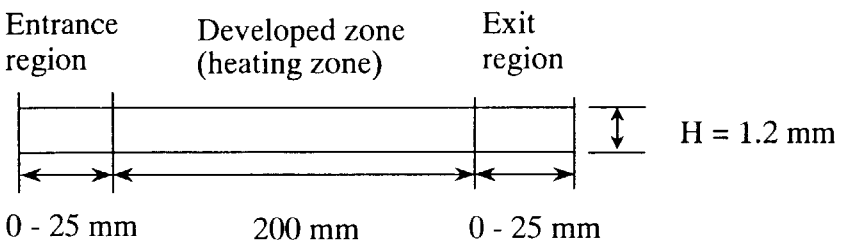

Equivalent hydraulic diameter, D_e = 4(W × H) / 2(W+H)
= 2 H, if W>> H
= 2.4 mm, where channel height, H = 1.2 mm

(3) Solution flow chart

The procedural steps how to obtain simulated friction and heat transfer data from the input values are given in a flow chart as shown below: At first, input values of flow velocity (u), channel height (H), and y^+ values, grid size of the computational geometry were fixed. After fixing grid size, fluid properties, boundary conditions and solution parameters were given as the input data of a analysis CFD-code, Star-CD. After running the STAR-CD interactively, local parameters such as, surface, bulk temperatures, and pressure drop data were obtained. From pressure drop, friction data were evaluated and then compared with the reference-Blasius one. Similarly, from local surface and bulk temperature data, local heat transfer coefficient consequently local Nusselt number were evaluated and then compared with the reference-Dittus-Boelter (D-B) one.

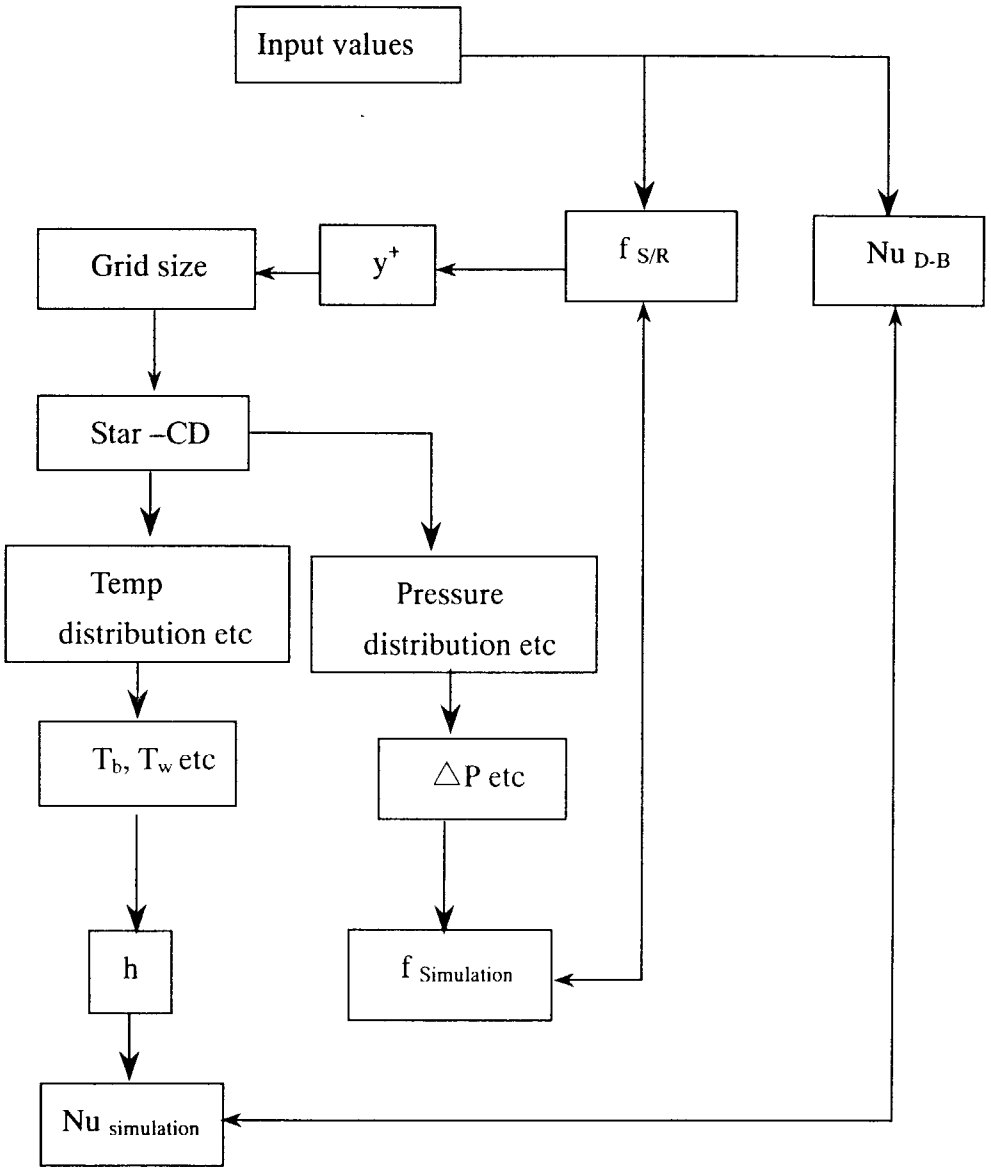

4.2 Governing equation

The three-dimensional Reynolds Averaged Navier-Strokes and energy equations along with the eddy viscosity concept are solved by the Star-CD to describe the incompressible flows in the computational domain. These equations are written in a Cartesian tensor form as shown below;

(1) Continuity equation

$$\frac{\delta u_i}{\delta x_i} = 0 \tag{1}$$

(2) Momentum equation

$$\rho \frac{\delta u_i}{\delta t} + \rho u_j \frac{\delta u_i}{\delta x_j} = -\frac{\delta P}{\delta x_i} + \mu \frac{\delta}{\delta x_j}\left(\frac{\delta u_i}{\delta x_j} + \frac{\delta u_j}{\delta x_i}\right) + \frac{\delta \tau_{i,j}}{\delta x_j} \tag{2}$$

Where j = x, y, z and i = x, y, z

(3) Energy equation

$$\rho \frac{\delta T}{\delta t} = \frac{\delta}{\delta x_i}\left[(\alpha + \alpha_t)\frac{\delta T}{\delta x_i}\right] \tag{3}$$

Where turbulent dynamic thermal diffusivity α_t are given by

$$\alpha_t = \frac{\mu_t}{\mathrm{Pr}_t} \tag{4}$$

The models chosen were the high-Re-number form of the Standard $k-\varepsilon$ and RNG $k-\varepsilon$. Constant thermo-physical properties were assumed, and natural convection is excluded as $(\mathrm{Gr}/\mathrm{Re}^2) < 0.0002$ where Gr and Re are the Grashof and the Reynolds numbers respectively.

(4) Standard $k-\varepsilon$ high-Re-number model equations

The turbulent kinetic energy (k) and its dissipation rate (ε) are computed from the standard $k-\varepsilon$ model of Launder and Spalding where the standard $k-\varepsilon$ model is based on the Boussinesq approximation. The modeled transport equations for turbulent kinetic energy (k) and dissipation (ε) are expressed for steady state, incompressible

flow, linear contribution, and negligible buoyancy effect as:

$$\frac{\delta}{\delta x_i}(\rho u_i k - \frac{\mu_{eff}}{\delta_k}\frac{\delta k}{\delta x_i}) = \mu_t P - \rho\varepsilon \tag{5}$$

$$\frac{\delta}{\delta x_i}(\rho u_i \varepsilon - \frac{\mu_{eff}}{\delta_\varepsilon}\frac{\delta \varepsilon}{\delta x_i}) = C_{\varepsilon 1}\frac{\varepsilon}{k}[\mu_t P] - C_{\varepsilon 2}\rho\frac{\varepsilon^2}{k} \tag{6}$$

$$\mu_t = c_\mu \rho k^2/\varepsilon \tag{7}$$

Where P denotes the production rate of kinetic energy, k , which is given by:

$$P = 2S_{ij}\frac{\delta u_j}{\delta x_i} \tag{8}$$

$$S_{ij} = \frac{1}{2}(\frac{\partial u_i}{\partial x_j} + \frac{\partial u_j}{\partial x_i}) \tag{9}$$

And

$$\mu_{eff} = \mu + \mu_t \tag{10}$$

(5) Standard RNG $k-\varepsilon$ high-Re-number model equations

The RNG (renormalization group) model is an alternative to the standard $k-\varepsilon$ model for high-Re-number flows. The model, which derives from a renormalization group analysis of the Navier-Stokes equations, differs from the standard model only through a modification to the equation for ε, except for using a different set of model constants. This model does not include compressibility or buoyancy effects.

$$\frac{\delta}{\delta x_i}(\rho u_i \varepsilon - \frac{\mu_{eff}}{\delta_\varepsilon}\frac{\delta \varepsilon}{\delta x_i}) = C_{\varepsilon 1}\frac{\varepsilon}{k}[\mu_t P] - C_{\varepsilon 2}\rho\frac{\varepsilon^2}{k} - \frac{C_\mu \eta^3(1-\eta/\eta_0)\rho\varepsilon^2}{1+\beta\eta^3} \tag{11}$$

where

$$\eta = 2(S_{ij}S_{ij})^{0.5}\frac{k}{\varepsilon} \tag{12}$$

and η_0 and β are additional empirical model constants given in the **Table 2.**
The constants appearing in Eqs. (5), (6), and (11) take values in the Table 2, which are

taken from Launder et al. [43].

4.3 Major Feature of Turbulent Model

(1) Standard $k-\varepsilon$ high-Re-number turbulent model

(i) With use of wall functions
(ii) Not valid in the region within the layer where molecular and turbulence effects are of comparable magnitude
(iii) Need not to employ a fine computational mesh within the layer

(2) Standard RNG $k-\varepsilon$ high-Re-number turbulent model

(i) Renormalization Group (RNG)
(ii) Improved version of the standard $k-\varepsilon$ turbulence model
(iii) With use of wall functions

(a) Wall functions

(i) Wall functions are well-known algebraic formulas, which represent the distribution of velocity, temperature, turbulent kinetic energy and its dissipation rate within the turbulent boundary layers that form adjacent to the wall.
(ii) They allow the boundary layer to be bridged by a single cell.
(iii) They are often used to bypass the necessity of detailed numerical treatment and the uncertain validity of a turbulence model.
(iv) Wall functions are an economic way of representing the turbulent boundary layers (hydrodynamic + thermal) in turbulent flow calculations.
(v) Wall functions to be effective, while the dimensionless normal distance, $y^+ = y\,u^*/\upsilon$ from the wall must not be too small or too large. Generally, y^+ range = 30 ~ 150 is used [55].

4.4 Boundary conditions

(1) Entrance

Hydro-dynamically developed uniform flow distribution and a uniform temperature T_o are assumed at the inlet of the channel in the present study. The inlet velocity, turbulent kinetic energy, k and its dissipation, ε profiles are obtained from a calculation of two-dimensional turbulent channel flow.

(2) Exit

At the outlet the stream wise gradients of all variables are set to be zero.

$$\frac{\delta f}{\delta x}=0; \quad f=\{u,v,k,\varepsilon,T\} \tag{13}$$

(3) Symmetry

At the symmetry planes, the normal velocity component and the normal derivatives of all other variables are set to be zero:

$$\frac{\delta f}{\delta z}=0; \quad f=\{u,v,k,\varepsilon,T\} \tag{14}$$

(4) Wall Boundaries

The wall functions proposed by Launder and Spalding, which are a linear–law relationship when $y_n^+ < 11.6$ and a log-law relationship when $y_n^+ > 11.6$ are used to prescribe the boundary conditions along the channel walls. The wall functions are applied in terms of diffusive wall fluxes. For the wall-tangential moment, the wall-shear stress is specified as:

$$\tau_w = \frac{\rho u_p C_\mu^{1/4} k_p^{1/2} \kappa}{\ln(E y^+)} \tag{15}$$

Where the wall functions constant, E = 9.0, $\kappa = 0.42$ and the non-dimensional wall distance y^+ is defined as:

$$y^+ = \frac{\rho y_p C_\mu^{1/4} k_p^{1/2}}{\mu} \tag{16}$$

The subscript, p, refers to node-point of the first grid adjacent to the wall. The production rate of k and the averaged dissipation rates over the near-wall cell for the k equation as well as the value of ε at the point p are computed respectively from following equations:

$$G_p = \tau_w \frac{u_p}{y_p} \tag{17}$$

$$\bar{\varepsilon} = \frac{1}{y_p}\int_0^{y_p} \varepsilon \, dy = \frac{C_\mu^{3/4} k_p^{3/2}}{\kappa y_p} \ln(E y^+) \tag{18}$$

$$\varepsilon_p = C_\mu^{3/4} \frac{k_p^{3/2}}{\kappa y_p} \tag{19}$$

For the temperature boundary condition, the heat flux to the wall is derived from the thermal wall function:

$$q_w = \frac{(T_w - T_p)\, \rho C_p C_\mu^{1/4} k_p^{1/2}}{\mathrm{Pr}_t [\frac{1}{\kappa} \ln(E y^+) + P]} \tag{20}$$

Where the empirical P function is specified as:

$$P = \frac{\pi/4}{\sin(\pi/4)} (A/\kappa)^{1/2} (\frac{\mathrm{Pr}}{\mathrm{Pr}_t} - 1)(\frac{\mathrm{Pr}t}{\mathrm{Pr}})^{1/4} \tag{21}$$

No–slip conditions for the velocity and the wall conditions for the turbulence quantities are specified at all of the boundary surfaces, including the rib surfaces.

4.5 Numerical Procedures

The **Star-CD** is a powerful CFD tool for thermo-fluids analysis, which has been used by the authors in order to investigate the velocity and temperature fields in two-dimensional turbulent channel flows with smooth and transverse repeated ribs. Its computational algorithm employs the **SIMPLE** method proposed by Patankar and the control volume approach is adopted to solve the hydrodynamic equations using a finite difference scheme. The study examined the performance of three discretization schemes (given below) for convection for the standard $k-\varepsilon$ and RNG$k-\varepsilon$ model solutions:

1. Upwind differencing scheme (UD)(First order differencing scheme)
2. Self-filtered central differencing scheme(SFCD)(Second order differencing scheme)
3. Quadratic upstream interpolation of convection kinematics scheme (QUICK) (Third order differencing scheme)

No distinguishable results were found among these. The convergence criterion used in

this computation is the value of mass flux residuals (mass flow). The under-relaxation factors for the velocity, the pressure, the turbulent kinetic energy, and the energy dissipation rate are set to be 0.7, 0.2, 0.7, and 0.95, respectively. The number of the iterations quite depends on the Reynolds number, grid sizes, and geometric parameters.

5. Computational Results and Discussion

5.1 Frictional pressure drop performance

To see the effect of grid size on frictional pressure drop and heat transfer, analyses were performed at different computational geometry's based on dimensionless distance (y^+) and the Reynolds number (Re). To account for the near-wall effects in the standard $k-\varepsilon$, RNG$k-\varepsilon$ models, the wall functions were used. This required the first interior grid point to be at a distance $y^+ > 11.5$ from the wall and required modifying the diffusion coefficient at the wall to satisfy the law of the wall relationship. To determine the grid size of the computational geometry of a smooth channel, a boundary layer thickness equation was used. The equation is given as:

$$y = \frac{D_e}{\mathrm{Re}} \sqrt{\frac{2}{f_{S/R}}}\, y^+ \tag{22}$$

In simplified form, we have the dimensionless distance,

$$y^+ = 0.0993\ \mathrm{Re}^{0.875}\ (y / H), \tag{23}$$

To verify the ability of the wall functions for the standard $k-\varepsilon$, RNG$k-\varepsilon$ models, three sets of y^+ values have been taken as 45, 22 and 15, respectively. It must be mentioned here that the Star-CD calculates half of the y^+ value in the computation. Generally y^+ is the total dimensionless distance of each cell of a computational geometry. However in Star-CD calculations, y^+ lies at the center of each cell. Smooth surface pressure drop and heat transfer were computed at channel height of 1.2 mm for the Reynolds number range of 7,000 to 22,000. One of the computational grids along with velocity magnitude of a smooth narrow channel for two-dimensional flow case is shown in **Fig. 10**. In the channel, the flow is entering at the inlet port with a uniform velocity of 3.5 m/s where the Reynolds number is 7,000 and the turbulent parameters (k & ε) are specified. The walls, which are parallel to the flow axis (X) are symmetric planes. The thermo-physical properties of water were taken at 15°C in the computation. The entire

computational flow length is 200 mm. Several computations of the standard $k-\varepsilon$ and RNG$k-\varepsilon$ models were performed with different mesh sizes, which are summarized in the **Table 3**. From Table 3, it is seen that the mesh size depends on the Reynolds number and dimensionless distance y^+ values. The mesh size must be adjusted when the Reynolds number was changed in order to keep a certain dimensionless distance y^+ value.

Based on this computational domain, frictional pressure drops and heat transfer performances were evaluated and compared with the reference one. The frictional pressure drops and heat transfer were calculated in the fully developed flow region. **Figures 11** and **12** show the pressure loss distribution in each segment along the flow channel. Each segment is at a distance of 5 mm. It is seen from these figures that fully developed flow was began at 70 mm ($L / D_e = 29$) from inlet of the flow length. The pressure drop was obtained within the fully developed flow regime of 60 mm (90 – 150) mm from the analytical results obtained by the Star-CD. The local pressure loss data, which were obtained by the standard $k-\varepsilon$ and RNG $k-\varepsilon$ models, are given in the **Table 4**. There are fourteen cases enlisted in the Table 4. Every three cases along with the last two cases is a particular Reynolds number where the mesh size is only the variable parameter. The frictional pressure loss data, which were calculated by the Blasius correlation, is also included for comparison. The calculated pressure drop quite depends on the grid size of a geometry. The calculated pressure drop agrees well with the Blasius prediction in the case of $y^+ = 22$. The prediction of pressure drop is almost the same as to $y^+ = 45$ but quite high in the case of $y^+ = 15$ ($y^+ < 11.5$). Because the grid size of $y^+ = 15$ was placed too close to the wall so that the ability of the wall functions was lost. The calculated frictional pressure drop was evaluated by the following equation:

$$f_{Simulation} = \Delta P \, D_e / (2 L \rho u^2) \tag{24}$$

And the reference one was predicted by the Blasius equation:

$$f_{Blasius} = 0.079 \, Re^{-0.25} \tag{25}$$

Figure 13 shows frictional pressure drop with respect to the dimensionless distance y^+ that was simulated by the Standard $k-\varepsilon$ and the RNG models under different Reynolds number. It is shown from this figure that frictional pressure loss agrees well with the reference one at $y^+ = 26$ (Star-CD, $y^+ = 13$) and both the standard $k-\varepsilon$ and the RNG models would be suitable to predict pressure loss characteristics in a smooth narrow channel geometry under water-flowing condition. **Figure 14** shows the discrepancy of

the frictional pressure loss performance between the standard $k-\varepsilon$ and the RNG models. No remarkable discrepancy was found in both models. This is due to insensitivity of grid sizes on pressure loss distribution between the two models at y^+ values of 45 and 22, respectively. To effective use of the wall functions, the y^+ value would be at least 11 in the Star-CD calculation. From **Figs. 11** to **14**, it is shown that frictional pressure drop performance has not agreed well with the reference one in the case of $y^+ = 15$ as the reason described earlier. It is evidenced from the calculated results that the standard $k-\varepsilon$ and RNG$k-\varepsilon$ turbulent models which use the wall functions are the most economical due to their simple treatment of the near-wall flow region, requiring minimal numerical resolution which saves grid points and hence computer storage and CPU time.

5.2 Heat Transfer Performance

The heat transfer performance was evaluated for the smooth narrow channel geometry. To predict the local heat transfer coefficient, the dimensionless parameter, the Nusselt number (Nu) has been used. The entire flow length is 200 mm as described above. The constant heat flux of 0.5 MW/m^2 from the bottom side of the computational geometry was assumed through the entire flow length. The local bulk and surface temperatures were taken at 100 mm from the inlet of the channel where the fully developed flow regime was obtained. Then the local heat transfer coefficient was calculated using the following equation:

$$h = \frac{q''_w}{(T_w - T_b)} \tag{26}$$

The local Nusselt number, Nu, calculated by Eq.(26) was compared with the Nusselt number for fully developed turbulent flow predicted by the Dittus-Boelter correlation, $Nu_{D\text{-}B}$.

$$Nu = h\, D_e / \lambda \tag{27}$$

$$Nu_{D\text{-}B} = 0.023\, Re^{0.8} Pr^{0.4} \tag{28}$$

Figure 15 shows the calculated surface and bulk temperature distributions along the flow direction. Fully developed flow region was obtained beyond 50 mm from the inlet where both the surface and bulk temperatures were parallel to each other. The calculated surface temperatures agree well with the reference one in the case of $y^+ = 45$ and 22,

respectively. At y^+ = 15, the surface temperatures are higher than those predicted by Dittus-Boelter (D-B) correlation and hence indicates low heat transfer coefficient. **Figure 16** shows the Nusselt number calculated for a smooth narrow channel by the Star-CD. Calculated Nu agrees well with the Dittus-Boelter as for using the wall functions, at y^+ = 45 and 22, respectively. The Nusselt number shown in Fig.16 were predicted by assuming local turbulent Prandtl number for Pr_t = 0.9 which is a well accepted value by all investigators. Although the local turbulent Prandtl number (Pr_t) is 0.94 by using the empirical equation of Pr_t proposed by Myong and Kasagi [56]. However there are some discrepancies amoung the constant values of Pr_t proposed by various investigators. The local variation of Pr_t in the various types of turbulent flows has not been fully resolved due to experimental difficulty and uncertainty involved in determining local turbulent Prandtl numbers.

Sensitivity of grid sizes between the two values of y^+ = 45 and 22 is not pronounced so far and hence the data reveals similar results. Calculated Nu number was quite far from that predicted by Dittus-Boelter correlation in the case of y^+ = 15. For these finer grid sizes, the node of a single cell was too close to the wall so that the ability of the wall functions was lost. It is well to note here that the wall functions used in connection with the standard model are usually applied in a region 22 < y^+ < 150. The standard $k-\varepsilon$ model would be better than the standard RNG$k-\varepsilon$ model for predicting heat transfer characteristics in a smooth narrow channel. **Figure 17** shows the comparative results of surface and bulk temperature changes while keeping zero (0) and 25 mm non-heating lengths at the entrance and exit regions of the analytical model. **Figure 18** shows its consequent entrance length effect on heat transfer performance for these surface and bulk temperature variations. The surface temperature estimated by Dittus-Boelter one becomes a slightly higher than the analytical one for the two cases as shown in Fig.17. Non-heating length region plays a little role as to persist full-developed flow region. Study showed that zero-non-heating length prevails lengthy entrance region than the having-non-heating length and the data are more scattered for the zero non-heating length case. From this figure it can be concluded that the total non-heating length = 50 mm predicts more smooth heat transfer distribution than the non-heating length = 0 due to less entrance region effect. However, it can also be concluded that there will be no major differences of heat transfer performances in the fully developed flow region even though variations of non-heating lengths of the analytical model. The calculated local heat transfer data for the zero non-heating length were obtained by the standard $k-\varepsilon$ and RNG$k-\varepsilon$ models that are given in the **Table 5**. Every three cases along with the last

two cases remains a particular velocity whereas there is a slight variation of the Reynolds number. This is due to the small variation of the bulk temperatures at 100 mm from the inlet of the analysis flow length.

Figure 19 shows the computational grid (17×2000) along with velocity magnitude of a rib-roughened narrow channel geometry. For the roughened geometry, the roughness height (k), spacing (p) are 0.2 and 2 mm, respectively and roughness spacing/height (p/k) is 10 according to experiments carried out by Islam et al.[4]. The calculated smooth and rib–roughened narrow channel pressure drop data obtained by the standard linear $k-\varepsilon$ turbulent model was compared with the available data measured by Islam et al. [4]. **Figure 20** shows the comparison results at Re = 7000. The analytical pressure loss results calculated by the standard $k-\varepsilon$ turbulent model were estimated about 5.6 times higher than the smooth one and nearly two times higher than the experimental one for the rib-roughened channel geometry. The reason for this large discrepancy between experimental and analytical pressure loss data of a rib-roughened surface is due to ignorance of recirculation and reattachment mechanism between the ribs in the wall functions approach. The systematic study on these differences needs further investigation by using a near wall turbulent model such as the low Reynolds number model.

6. Concluding Remarks

Heat transfer and pressure drop characteristics under fully developed turbulent water flow condition were analyzed numerically over a two-dimensional smooth narrow rectangular channel whose height is H = 1.2 mm. The channel configuration and water flow condition simulate forced convection cooling of a spallation target system components design such as a solid target and a proton beam window. The high-Re-number form of the standard $k-\varepsilon$ and RNG$k-\varepsilon$ models were used in the analyses. The heat transfer analyses of the smooth narrow water-flow channel were performed for the condition of uniform wall heat flux from one-side, for a range of Reynolds numbers from 7,000 to 22,000. The frictional pressure drop was evaluated in non-heating conditions of the flow channel.

As for heat transfer characteristics, the Nusselt number obtained by the standard $k-\varepsilon$ model agreed very well with the Dittus-Boelter correlation. However, the calculated pressure losses (y^+ = 22, 45) were found no significant effect on grid sizes for both models except y^+ = 15. The local heat transfer coefficients were taken in the fully developed region, which lies at mid-position of the analysis flow length. The pressure

drop was calculated between the distance of 60 mm (90 – 150) mm from the inlet of the channel. Heat transfer performances were affected by the computational grid sizes of a geometry. Heat transfer performances also vary over entrance length. The longer the non-heating length, the lesser is the entrance length region. The $k-\varepsilon$ high-Re-number turbulent models employing wall functions predicted more reliable and accurate results in the smooth narrow water-flow channel. In most high-Re-number flows, the wall functions approach is a practical option for the near-wall treatments for industrial flow analyses. The rib-roughened surface was claimed to be very high frictional pressure loss performance compared with the experimental one for the grid sizes of 17×2000. This is obvious due to not occur separation and reattachment mechanism between the ribs. The systematic study on rib-roughened channel flows needs further investigation.

Acknowledgements

In this study, the authors wish to express their sincere gratitude to the System Engineering group staff, Centre for Neutron Science (CENS), JAERI as to provide laboratory facilities to perform analytical studies. Special thanks are due to Mr. Masanori Kaminaga for his valuable comment and suggestions. To all, we are extremely grateful.

Nomenclature

A	Van Driest constant
C_μ C_1 C_2 C_3	turbulence models constants
C_p	specific heat at constant pressure
D_e	hydraulic equivalent diameter, $D_e = 4WH / 2(W+H) = 2H$ [W>>H]
E	Constant in logarithmic law of wall (E=9.0)
f	roughened friction factor
Gr	Grashof number, $Gr = \frac{g\,\beta\,D_e^{\,3}(T_w - T_b)}{\nu^2}$
h	forced convection heat transfer coefficient
H	channel height
k	rib height
k	turbulent kinetic energy, $k = \frac{1}{2}\overline{u_i}\,\overline{u_i}$
k^+	dimensionless turbulent kinetic energy, $k^+ = \frac{k}{u^{*2}}$

L	channel length
Nu	Nusselt number, Nu = h D_e / λ
p	rib spacing
P	pressure
P_k	production of turbulent kinetic energy
ΔP	pressure difference,
Pr	molecular Prandtl number, Pr = $C_p \ \mu / \lambda$
Pr_t	turbulent Prandtl number
q_w	wall heat flux
Re	Reynolds number, Re =$D_e \ u_m / \nu$
Re_y	ribs Reynolds number, $Re_y = \frac{y\sqrt{k}}{\nu}$
Re_t	turbulent eddy Reynolds number, $Re_t = \frac{k^2}{\nu \varepsilon}$
T	temperature
u	local axial fluid velocity
u*	friction velocity, $u^* = \left[\tau_w / \rho\right]^{1/2}$
W	channel width
y	local distance from the surface
y^+	dimensionless distance, y u* / ν
x_i, x_j	cartesian coordinates

Greek symbol

μ	molecular viscosity
μ_t	turbulent eddy viscosity
ν	kinematic viscosity
ε	dissipation of turbulent kinetic energy
ε^+	dimensionless dissipation rate, $\varepsilon^+ = \frac{\nu\varepsilon}{u^{*4}}$
η_0 δ_k δ_ε	turbulent model constants
β	turbulent model constant /thermal expansion coefficient
κ	Von Karman constant
α_t	turbulent thermal diffusivity, μ_t / Pr_t

α	molecular thermal diffusivity, $\lambda / \rho C_p$
α_a	helix angle
ρ	density
τ	wall shear stress
λ	thermal conductivity

Subscripts

b	bulk
cal	calculated
D-B	Dittus-Boelter
H	heated
i, j	Einstein constant
p	cell center-point
S/R	smooth/rough
t	turbulent
eff	effective
w	wall

References

[1] Hino, R., et al., Spallation Target Development at JAERI, 14th Meeting of the Int. Collaboration on Advanced Neutron Sources (ICANS), (U.S.A) June14-19 (1998).

[2] Kaminaga, M., Terada, A., Haga, K., Kinoshita, H., and Hino, R., Thermal-Hydraulic Design of Cross-Flow Type Mercury Target for JAERI/KEK Project, 15th Meeting of the Int. Collaboration on Advanced Neutron Sources (ICANS), (Japan) Nov.6-9 (2000).

[3] Teraoku, T., Kaminaga, M, Terada, A., Ishikura, S., Kinoshita, H., and Hino, R., Conceptual Design of Proton Beam Window, 15th Meeting of the Int. Collaboration on Advanced Neutron Sources (ICANS), (Japan) Nov.6-9 (2000).

[4] Islam, M. S., Hino, R., Haga, K., Monde, M., and Sudo, Y., Experimental Study on Heat Transfer Augmentation for High Heat Flux Removal in Rib-Roughened Narrow Channels, Journal of Nuclear Science and Technology, Vol.35, No.9, pp.671-678 (1998).

[5] Kalinin, E. K., Drietser, G. A., Yarkho, S. A., and Kusminov, V. A., The Experimental Study of the Heat Transfer Intensification Under Conditions of Forced One-and

Two-Phase Flow in Channels, in Augmentation of Convective Heat and Mass Transfer, ASME Symposium Volume, pp.80-90 (1970).

[6] Nikuradse, J., Laws of Flow in Rough pipes, VDI Forsch., 361 (1933). English Translation. NACA TM-1292, (1965).

[7] Dipprey, D. F and Sabersky, R. H., Heat and Momentum Transfer in Smooth and Rough Tubes at Various Prandtl Numbers. J. Heat and Mass transfer 6, pp.329-353 (1963).

[8] Gee, D. L., and Webb, R. L., Forced Convection Heat Transfer in Helically Rib-Roughened Tubes, Int. J. Heat Mass Transfer,Vol.23, pp.1127-1136 (1988).

[9] Withers, J. G., Tube-Side Heat Transfer and Pressure drop for Tubes Having Helical Internal Ridging with Turbulent/ Transitional Flow of Single-Phase Fluid. Part1. Single-Helix Ridging, Heat Transfer Eng.,Vol.2 , No.1, pp.48-58 (1980).

[10] Li, et al., Investigation on Tube-Side Flow Visualization, Friction Factors and Heat Transfer Characteristics of Helical-Ridging Tubes, in Heat Transfer Proc.7th Int. Heat Transfer Conf., Vol.3, pp.75-80 (1982).

[11] Nakayama, M., Takahashi, K., and Daikoku, T., Spiral Ribbing to Enhance Single-Phase Heat Transfer Inside Tubes, ASME-JSME Thermal Engineering Joint Conf., pp.365-372 (1983).

[12] Han, J. C. et al., An Investigation of Heat Transfer and Friction for Rib-Roughened Surfaces, Int. J. Heat Mass Transfer, Vol.21, pp.1143–1156 (1978).

[13] Liou,-M. T. and Hwang,-J. J., Effect of Ridge Shapes on Turbulent Heat Transfer and Friction in a Rectangular Channel, Int. J. Heat Mass Transfer, Vol.36, No.4, pp.931–940 (1993).

[14] Webb, R. L., Eckert, E. R. G., and Goldstein, R. J., Heat Transfer and Friction in Tubes with Repeated-Rib Roughness, Int. J. Heat Mass Transfer, Vol.14, pp.601-617 (1971).

[15] Chiou, J. P., Augmentation of Forced Convection Heat Transfer in a Circular Tube Using Spiral Spring Inserts, ASME Paper 83-HT-38., (1983).

[16] Zhang, Y. F., Li, F. Y., and Liang, Z. M., Heat Transfer in Spiral-Coiled-Inserted Tubes and its Applications, in Advances in Heat Transfer Augmentation and Mixed Convection, ASME HTD-Vol.169, pp.31-36 (1991).

[17] Ravigururajan, T. S., and Bergles, A. E., Study of Water-Side Enhancement for Ocean Thermal Energy Conversion Heat Exchangers, Final Report, College of Engineering, Iowa State University, Ames (1986).

[18] Yoshitomi, H., Oba, K., and Arima, Y., Heat Transfer and Pressure Drop in Tubes

with Embossed Spiral, Thermal and Nuclear Power (in Japanese), Vol.26, pp. 171-182 (1976).

[19] Berger, F. P., and Whitehead, A. W., Fluid Flow and Heat Transfer in Tubes with Internal Square Rib Roughening, J. Br. Nuclear Energy Soc., Vol. 20, No.2, pp.153-160, pp.605-613 (1977).

[20] Migai, V. K., and Bystrov, P. G., Heat Transfer in Profiled Tubes, Thermal Eng., Vol.28, pp.178-182 (1981).

[21] Bolla et al., Heat Transfer and Pressure Drop Comparison in Tubes with Transverse Ribs and with Twisted Tapes, Energia Nucleare, No.20, pp. 605-613 (1973).

[22] Ganeshan, S., and Rao, M. R., Studies on Thermohydraulics of Single and Multi-Start Spirally Corrugated Tubes for Water and Time-Independent Power Law Fluids, Int. J. Heat Mass Transfer, Vol.25, No.7, pp. 1013-1022 (1982).

[23] Gupta, R. H., and Rao, M. R., Heat Transfer and Frictional Characteristics of Spirally Enhanced Tubes for Horizontal Condensers, in Advances in Enhanced Heat Transfer, ASME Symposium Volume, pp.11-21 (1979).

[24] Nunner, W., Heat Transfer and Pressure Drop in Rough Tubes, UK Atomic Energy Authority, Harwell, Atomic Energy Research Establishment Lib/ Trans.786 (1956).

[25] Sams, E. W., Heat Transfer and Pressure-Drop Characteristics of Wire-Coiled Type Turbulence Promoters, TID-7529, Pt.1, Book2, Nov.1957, pp.390-415 (1956).

[26] Kumar, P., and Judd, R. L., Heat Transfer with Coil Wire Turbulence Promoters, Can. J. Chem. Eng., Vol. 48, pp.378-393 (1970).

[27] Novozhilov, J. F., and Migai, V. K., Intensifying Convective Heat Transfer within Tubes by Means of Induced Roughness, Teploenergetika, Vol.11, No.6, pp.60-63 (1981).

[28] Snyder, P. H., Intensifying Convective Heat Transfer for Moderate Prandtl Number and Reynolds Number Flows within Tubes by Means of Wire Coil Type Turbulent Promoters, Westinghouse Research Laboratories Report72-1E9-RELIQ-R1 (1972).

[29] Sethumadhavan, R., and Rao, M. R., Turbulent Flow Heat Transfer and Fluid Friction in Helical-Wire-Coil-Inserted Tubes, Int. J. Heat Mass Transfer, Vol.26, pp.1833-1845 (1983).

[30] Molloy, J., Rough Tube Friction Factors and Heat Transfer Coefficients in Laminar and Transition Flow, UKAEA AERE-R5415 (1967).

[31] Ravigururajan, T. S., General Correlations for Pressure Drop and Heat Transfer for Single-Phase Turbulent Flow in Ribbed Tubes, Ph. D. Thesis, Iowa State University, Ames, (1986).

[32] Mehta, M. H., and Rao, M. R., Heat Transfer and Frictional Characteristics of Spirally Enhanced Tubes for Horizontal Condensers, in Advances in Enhanced Heat Transfer, ASME Symposium Volume, pp.11-22 (1979).

[33] Cunningham, J., and Milne, H. N., The Effect of Helix Angle on the Performance of Rope Tubes, Proc. Sixth Int. Heat Transfer Conf., Vol.2 pp.601-605 (1978).

[34] Mendes, P. R. S., and Mauricio, M. H. P., Heat Transfer, Pressure Drop, and Enhancement Characteristics of the Turbulent Through Internally Ribbed Tubes, ASME HTD Vol.82, pp. 15-22 (1987).

[35] Yampolsky, J. S., Libby, P. A., Launder, B. E., and LaRue, J. C., Fluid Mechanics and Heat Transfer Spiral Fluted Tubing, Final Report, G A Technologies Report GA-A17833, (1984).

[36] Scaggs, W. F., Taylor, P. R., and Coleman, H. W., Measurement and Prediction of Rough Wall Effects of Friction Factor in Turbulent Pipe Flow, Report TFD-88-1, Mississippi State University (1988).

[37] Newson, I. H., and Hodgson, T.D., The Development of Enhanced Heat Transfer Condenser Tubing, Desalination, Vol.14, pp.291-323 (1974).

[38] Sutherland, W. A., and Miller, C. W., Heat Transfer to Super Heater Steam-I, Improved Performance with Turbulent Promoters, USAEC Report, GEAP-4749 (1964).

[39] Smith, J. W., and R. A. Gowen, Heat Transfer Efficiency in Rough Pipes at High Prandtl Number, AIChE J., Vol.11, pp.941-943 (1965).

[40] Takahashi, K., Kayama, W., and Kuwahara, H., Enhancement of Forced Convective Heat Transfer in Tubes Having Three-Dimensional Spiral Ribs, Trans. JSME, Vol. 51, pp.350-355 (1985).

[41] Obot, N. T., and Esen, E. B., Heat Transfer and Pressure Drop for air Flow Through Enhanced Passages, Report DOE/CE/90029-8, Fluid Mechanics, Heat, and Mass Transfer Laboratory Report, FHMT Report 007, Clarkson University, NY (1992).

[42] Bejan, A., Convective Heat Transfer, John Wiley & Sons, New York (1989).

[43] Launder, B. E., and Spalding, D. B., The Numerical Computation of Turbulent Flows, Computer Methods in Applied Mechanics and Engineering, Vol.3, pp.269-289 (1974).

[44] Lewis, M. J., An Elementary Analysis for Predicting the Momentum and Heat Transfer Characteristics of a Hydraulically Rough Surface, J. Heat Transfer Vol.97, pp.249-254 (1975).

[45] Lee, B. K., Cho, N. H., and Choi, Y. D., Analysis of Periodically Fully Developed

Turbulent Flow and Heat Transfer by $k-\varepsilon$ Equation Model in Artificially Roughened Annulus, Int. J. Heat Mass Transfer Vol.31, pp.1797-1806 (1988).

[46] Patankar, S.V., Liu, C., and Sparrow, E.M., Fully Developed Flow and Heat Transfer in Ducts Having Stream wise-Periodic Variations of Cross-Sectional Area, Trans. ASME J. Heat Transfer Vol.99, pp.180-186 (1977).

[47] Liou, T. M., Hwang, D. C., and Kao, C. F., Computations of Turbulent Flow and Heat Transfer Enhancement in Channel with a Pair of Turbulence Promoters, 3rd Int. Symposium on Transport Phenomena in Thermal Control, Taipei, Taiwan (1988).

[48] Durst, F., and Rastogi, A. K., Turbulent Flow over Two-Dimensional Fences, Turbulent Shear Flows2, Bradbury et al., eds., Berlin, Springer-Verlag., pp.218-231 (1980).

[49] Yap, C., Turbulent Heat and Momentum Transfer in Recirculating and Impinging Flows, Ph.D. Thesis, Faculty of Tech., University of Manchester, U.K. (1987)

[50] Jones, W. P., and Launder, B. E., The Calculation of Low-Reynolds Number Phenomena with a Two-Equation Model of Turbulence, Int. J. Heat Mass Transfer Vol.16, pp.1119-1130 (1972).

[51] Leschziner, M. A. and Rodi, W., Calculation of Annular and Twin Parallel Jets Using Various Discretization Schemes and Turbulence Model Variations, J. Fluid Engng Vol.103, pp.352-360 (1981).

[52] Benodekar, R. W. et al., Numerical Prediction of Turbulent Flow over Surface-Mounted Ribs, AIAA J. Vol. 23(3), pp.359-366 (1985).

[53] Chung, M. K. et al., Curvature Effect on Third-Order Velocity Correlations and Its Model Representation, Physics Fluids Vol.30 (3), pp.626-628 (1987).

[54] Park, S. W., and Chung, M. K., Curvature-Dependent Two-Equation Model for Prediction of Turbulent Recirculating Flows, AIAA J. Vol.27, pp.340-344 (1989)

[55] Computational Fluid Dynamics Software, Star-CD (Methodology Volume) 1999.

[56] Myong, H. K., Kasagi, N., and Hirata, M., Numerical Prediction of Turbulent Pipe Flow Heat Transfer for Various Prandtl Number Fluids with the Improved $k-\varepsilon$ Turbulence Model, JSME Int. Journal, Series II, Vol.32, No.4, pp.613-622 (1989).

Table 1 Investigations Cited in This Study [a]

Study	Tubes tested	Type	Fluid	Expt. condition	f	N-ISO-f	HT
1. Kalinin [5]	10	ind.	Air	W. cooled	10	0	10
2. Gee and Webb [8]	3	rib	Air	E.H.	3	3	3
3. Withers [9]	13	ind.	W	T=Const	13	0	13
4. Li [10]	20	ind.	W	E.H.	20	0	20
5. Nakayama [11]	6	ind.	W	E.H.	6	0	6
6. Webb [14]	5	rib	A,W	E.H.	5	5	5
7. Chiou [15]	15	coil	oil	W. cooled	0	15	15
8. Zhang [16]	32	coil	Air	W. cooled	32	0	32
9. Ravigururajan [17]	4	ind.	W	E.H.	4	4	4
10. Yoshitomi [18]	18	ind.	W	E.H.	18	0	18
11. Berger [19]	3	rib	Air	E.H.	3	0	3
12. Migai [20]	10	ind./fl	Air	T=Const	10	0	10
13. Bolla [21]	1	rib	He,N_2	W. heated	1	0	1
14. Ganeshan [22]	7	ind.	W	W. heated	7	0	7
15. Gupta [23]	5	ind.	W	W. heated	5	0	5
16. Nunner [24]	4	rib	Air	W. heated	4	0	4
17. Sams [25]	13	coil	Air	E.H.	13	0	13
18. Kumar [26]	14	coil	W	E.H.	0	14	14
19. Novozhilov [27]	10	coil	Air	E.H.	10	0	10
20. Snyder [28]	11	coil	W	E.H.	11	0	11
21. Sethumadhavan[29]	8	coil	W	W. heated	8	8	8
22. Molloy [30]	1	coil	Air	E.H.	1	0	1
23. Ravigururajan [31]	5	coil	Air	W. cooled	5	0	5
24. Mehta [32]	8	ind.	W	W. heated	8	0	8
25. Cunningham [33]	3	ind.	W	W. heated	3	0	0
26. Mendes [34]	3	rib	W	Sublimation	0	3	3
27. Yampolsky [35]	4	flute	W	W. heated	0	1	1
28. Scaggs [36]	3	3d	W	ISO	3	0	0
29. Newson [37]	24	flute	W	W. heated	0	24	24
30. Sutherland [38]	1	rib	Stm	E.H.	0	1	1
31. Smith [39]	2	3d	A,W, G	E.H.	0	2	2
32. Takahashi [40]	3	3d	W	E.H.	2	0	2
33. Obot [41]	24	all	Air	E.H.	4	24	24

[a]E.H=Electrical heating, A= air, G= glycerin, Stm=steam, W=water, ISO=isothermal, HT=heat transfer

Table 2 Constants in Turbulent Equations

Keyword	Symbol	Default	Comments
CAPPA	κ	0.42	Von Karman constant
CMU	C_μ	0.09	Constant in eddy viscosity formula
		0.085	C_μ in RNG model
C1	$C_{\varepsilon 1}$	1.44	Constant in ε equation
		1.42	Constant in RNG model
C2	$C_{\varepsilon 2}$	1.92	Constant in ε equation
		1.68	Constant in RNG model
BETARG	β	0.012	Constant in RNG model
ETAORG	η_o	4.38	Constant in RNG model
K	δ_k	1.0	Turbulent Prandtl number for K
		0.719	Turbulent Prandtl number for K in RNG model
ε	δ_ε	1.22	Turbulent Prandtl number for ε for $k-\varepsilon$ Turbulence model
		0.719	Turbulent Prandtl number for ε in RNG model

Table 3 Computational Grid Size of a Smooth Narrow Channel Height, H=1.2 mm

Case No.	Re	u (m / s)	Mesh No.	y^+_{cal}	Y (mm) (1mesh- size)	y^+ Star-CD (STD. $\kappa-\varepsilon$)
i.	7000	3.35	5	45	0.23	22.55
ii.			10	22	0.11	11.22
iii.			15	15	0.078	8.32
iv.	9000	4.3	6	45	0.188	23.34
v.			13	22	0.092	10.77
vi.			19	15	0.062	8.16
vii	12000	5.73	8	45	0.146	22.45
viii.			17	22	0.071	10.61
ix.			25	15	0.048	7.97
x.	16000	7.65	11	45	0.11	20.97
xi.			22	22	0.055	10.55
xii.			32	15	0.037	7.97
xiii.	22000	10.52	14	45	0.086	21.75
xiv.			28	22	0.042	10.82

Table 4 Calculated Frictionnal Pressure Loss Data in a Smooth Narrow Channel

Fully developed flow region, L = (90 -150) mm

Channel height, H=1.2 mm, Non heating condition, (2 - D Model)

Case No.	Re	U(m/s)	Mesh No.	y(mm)	*1 Y^+_{Cal}	*2 $Y^+_{STD.\kappa-\varepsilon}$	*3 $Y^+_{RNG/\kappa-\varepsilon}$	$f_{STD.\kappa-\varepsilon}$	$f_{RNG/\kappa-\varepsilon}$	$f_{Blasius}$
i.	7000	3.35	5	0.23	45	22.55	21.6	0.0088	0.0082	0.0086
ii.			10	0.11	22	11.22	11.02	0.0088	0.0086	
iii.			15	0.08	15	8.32	8.21	0.0112	0.011	
iv.	9000	4.3	6	0.19	45	23.34	22.36	0.0083	0.0076	0.0081
v.			13	0.09	22	10.77	10.65	0.0083	0.0082	
vi.			19	0.06	15	8.16	8.03	0.01	0.01	
vii.	12000	5.73	8	0.15	45	22.45	21.51	0.0076	0.007	0.0075
viii.			17	0.07	22	10.61	10.48	0.0078	0.0076	
ix.			25	0.05	15	7.97	7.83	0.0097	0.0095	
x.	16000	7.65	11	0.11	45	20.97	20.08	0.007	0.0065	0.007
xi.			22	0.05	22	10.55	10.41	0.0072	0.0071	
xii.			32	0.04	15	7.97	7.82	0.0089	0.0087	
xiii.	22000	10.52	14	0.08	45	21.75	20.83	0.0065	0.006	0.0065
xiv.			28	0.04	22	10.82	10.67	0.0065	0.0064	

Thermo-physical properties of water at 15 °C (Inlet)

Density, ρ = 999.12 kg /m^3

Viscosity, μ = 1146.83 $\times 10^{-6}$ Pa s

Specific heat, C_p = 4187.305 J /(kg K)

Thermal conductivity, λ = 0.5878 W/(m K)

Turbulent Prandtl Number, Pr_t = 0.9

Molecular Prandtl number , Pr = 8.06

Note:

*1 Assumed y^+ value

*2 Calculated y^+(STD. $\kappa-\varepsilon$) value by Star-CD

*3 Calculated y^+(RNG $\kappa-\varepsilon$) value by Star-CD

Table 5 Calculated Local Heat Transfer Coefficient Data in a Smooth Narrow Channel

(2-D Model)
Channel height, H =1.2 mm
Local values at 100 mm from inlet

Case No.	Re	U(m/s)	Mesh No.	y (mm)	Y^+_{Cal}	Y^+	T_w (K)	T_b (K)	f	$f_{Blasius}$	Nu	Nu_{D-B}
i.	7610	3.35	5	0.23	45	26(*25.07)	322.14(*323.81)	291.22(*291.22)	0.0086(*0.008)	0.0084	65.41(*62.06)	65.01
ii.	7620	3.35	10	0.11	22	13.34(*12.95)	322.18(*323.68)	291.26(*291.25)	0.0086(*0.008)	0.0084	65.4(*62.36)	65.04
iii.	7620	3.35	15	0.078	15	9.56(*9.49)	329.38(*329.69)	291.26(*291.27)	0.01(*0.0098)	0.0084	53.05(*52.63)	65.04
iv.	9600	4.3	6	0.188	45	26.3(*25.35)	316.21(*317.61)	290.52(*290.52)	0.0081(*0.0074)	0.0079	78.88(*74.44)	78.93
v.	10250	4.3	13	0.092	22	12.57(*12.1)	317(*318.28)	293.09(*291.25)	0.0077(*0.0072)	0.0078	84.15(*74.44)	80.74
vi.	9610	4.3	19	0.062	15	9.17(*9.09)	321.2(*290.56)	290.56(*290.56)	0.0096(*0.0094)	0.0079	66.13(*65.53)	78.95
vii.	12590	5.73	8	0.146	45	24.8(*23.88)	310.05(*311.62)	289.91(*289.9)	0.0075(0.0069)	0.0074	98.59(*93.51)	98.77
viii.	12600	5.73	17	0.071	22	11.82(*11.5)	310.7(*323.21)	289.93(*289.93)	0.0075(*0.0072)	0.0074	97.73(*90)	98.79
ix.	12600	5.73	25	0.048	15	8.77(*8.67)	313.6(*313.84)	289.93(*289.94)	0.0091(*0.0089)	0.0074	85.76(*84.93)	98.79
x.	16610	7.65	11	0.11	45	22.78(*21.92)	305.9(*306.8)	289.44(*289.45)	0.0069(*0.0064)	0.0069	123.5(*117.16)	123.9
xi.	16620	7.65	22	0.055	22	11.46(*11.22)	306.09(*315.48)	289.45(*289.46)	0.0069(*0.0067)	0.0069	122.16(*110)	124
xii.	16610	7.65	32	0.037	15	8.61(*8.49)	308.16(*308.36)	289.46(*289.46)	0.0085(*0.0083)	0.0069	108.7(*107.55)	124
xiii.	22580	10.52	14	0.086	45	23.23(*22.33)	301.86(*302.57)	289.06(*289.06)	0.0065(*0.0059)	0.0064	158.99(*150.63)	159.2
xiv.	22620	10.52	28	0.042	22	11.63(*11.34)	302.02(*309.66)	289.07(*289.07)	0.0064(*0.0061)	0.0064	157.14(*140)	159.4

Thermo-physical properties of water at 15 °C (Inlet)
Density, ρ = 999.12 kg /m^3, f (T)
Specific heat, C_p = 4187.30 J / (kg K) , f (T)
Thermal conductivity, λ = 0.5878 W/(m K) , f (T)
Turbulent Prandtl Number, Pr_t = 0.9
Molecular Prandtl Number , Pr = 8.06

Note : Non bracketed one ; calculated $\kappa-\varepsilon$ value by Star-CD
Bracketed asterick, * ; calculated RNG $\kappa-\varepsilon$ value by Star-CD

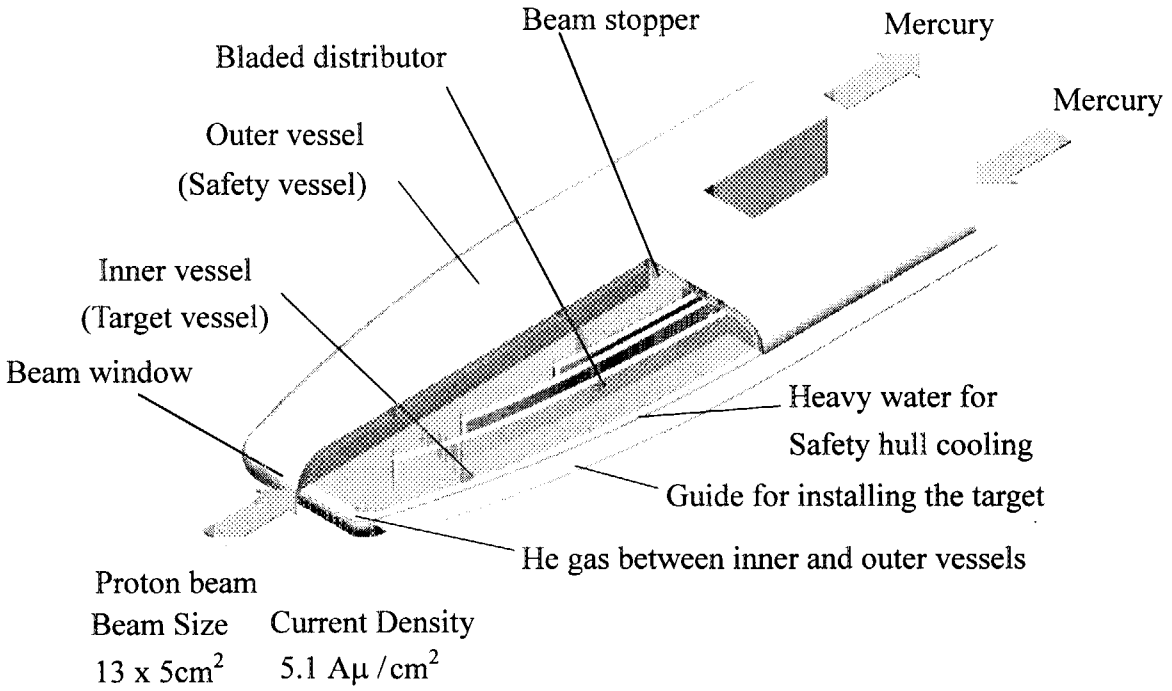

Fig. 1 Cross-Flow Type (CFT) Target with Safety Hull

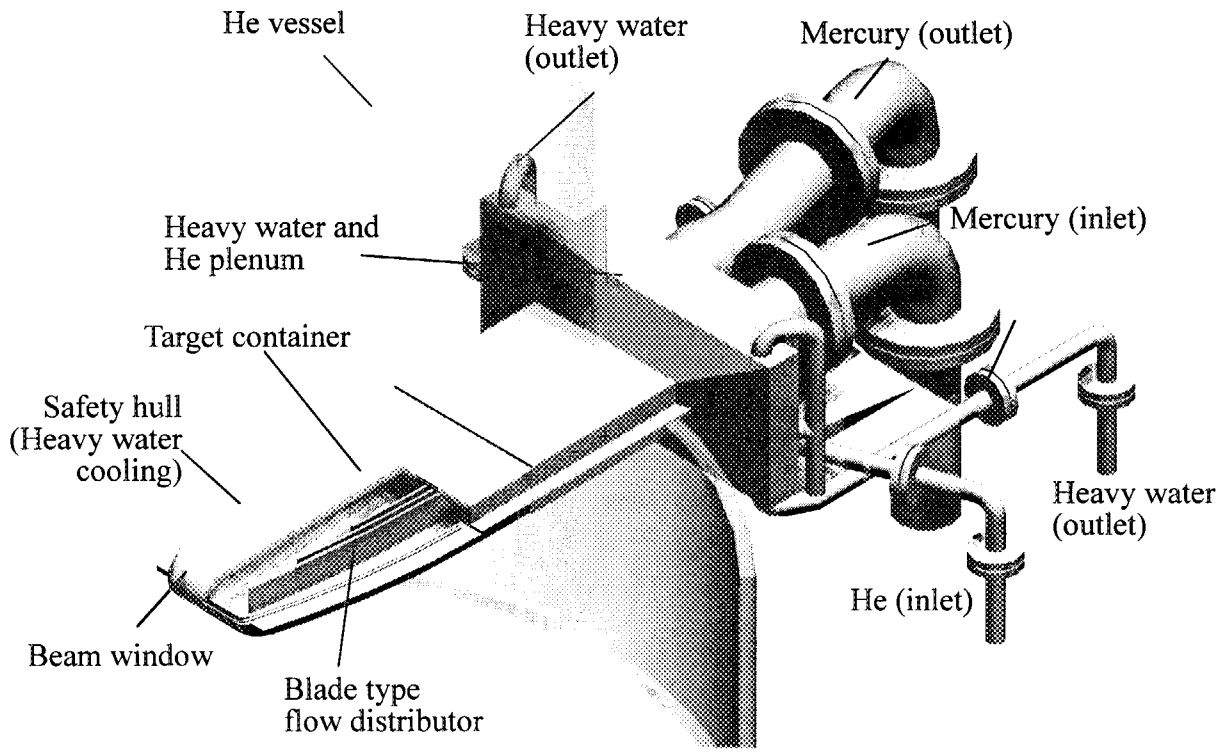

Material : SUS316L

Dimension : Target vessel 80 mm(height),200-500mm(width), Effective length 800mm

Safety hull 100 mm(height), 300-650mm(width), length 1500 mm

Fig. 2 Integrated Mercury Target with Safety Hull

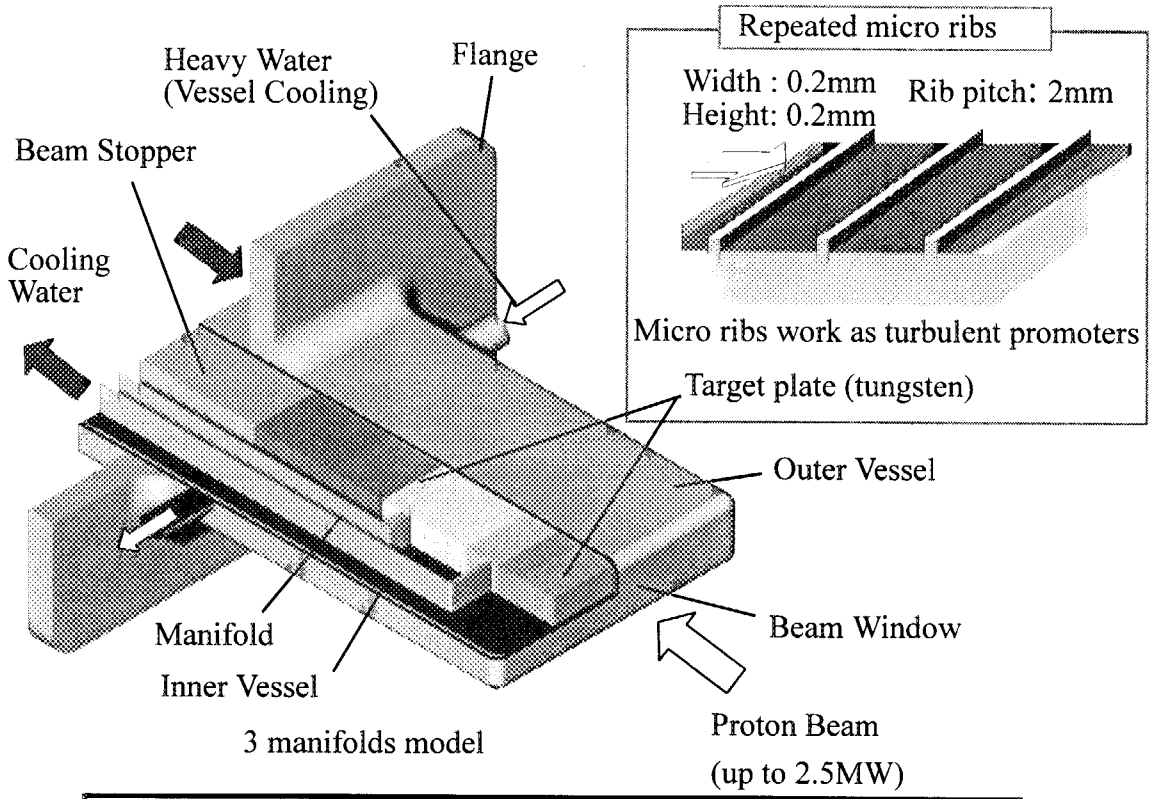

Fig. 3 Concept of Solid Target for 1MW and up to 2.5MW Operations

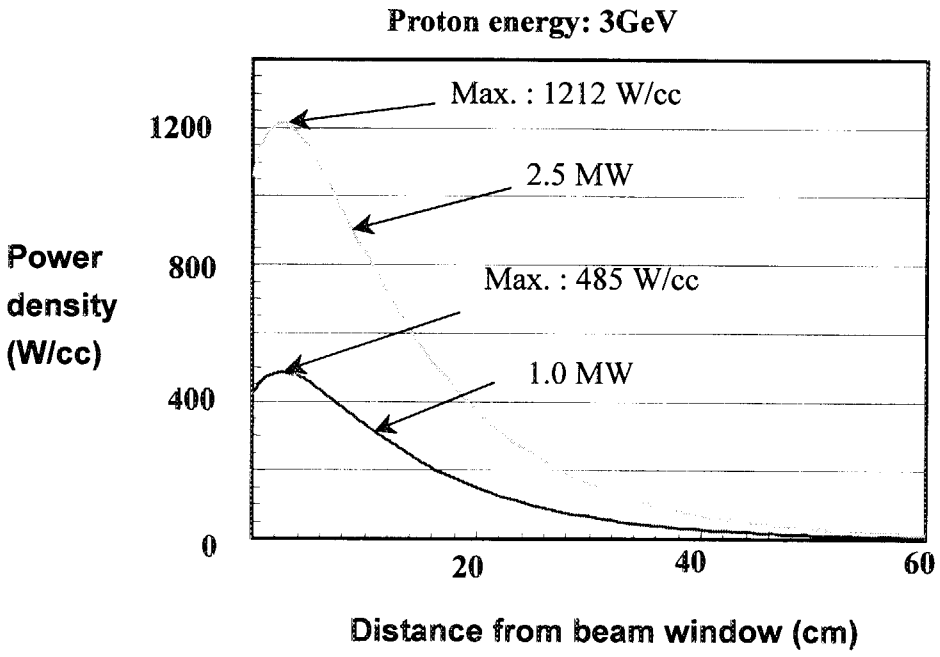

Fig. 4 Power Density of Solid Targets
(25% margin already included)

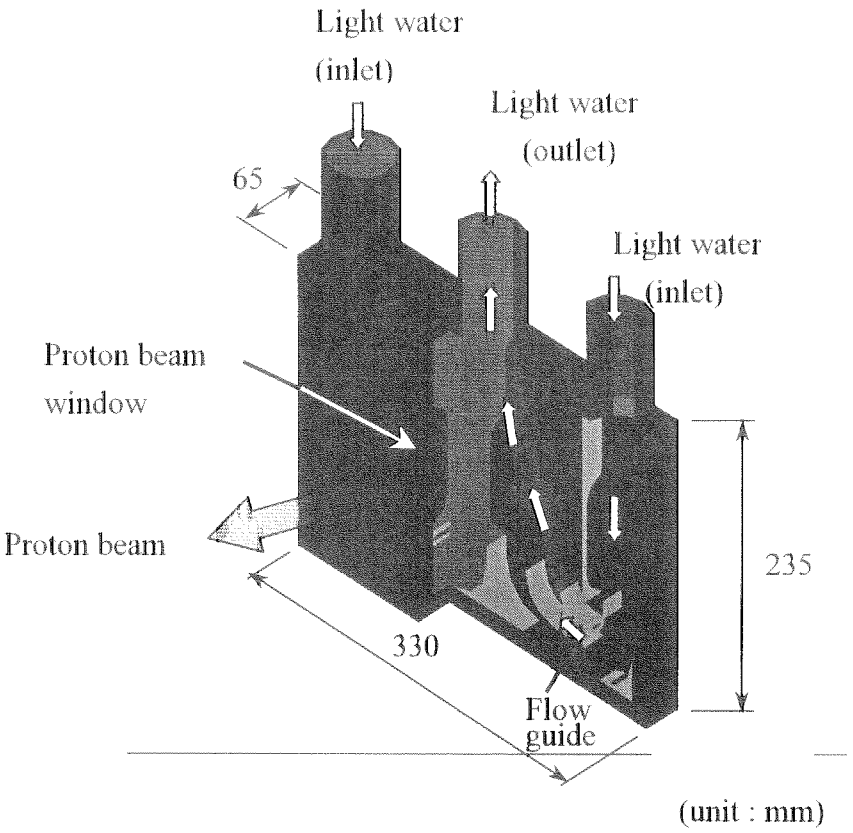

Fig. 5 Conceptual Design of a Proton Beam Window

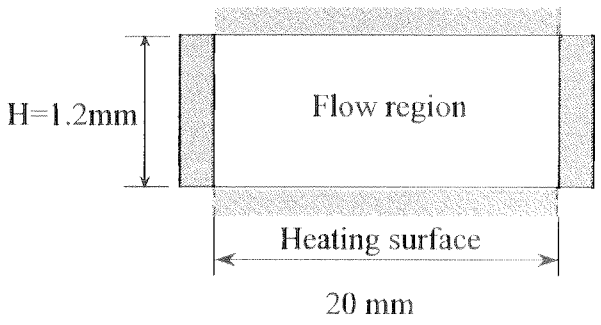

Fig. 6 Cross Section of Flow Channel

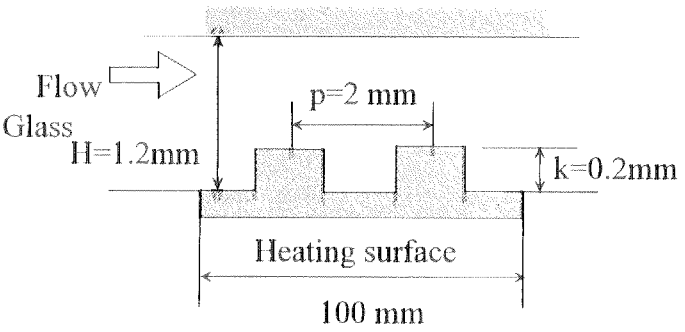

Fig. 7 Flow Channel With Rib-Roughened Surface

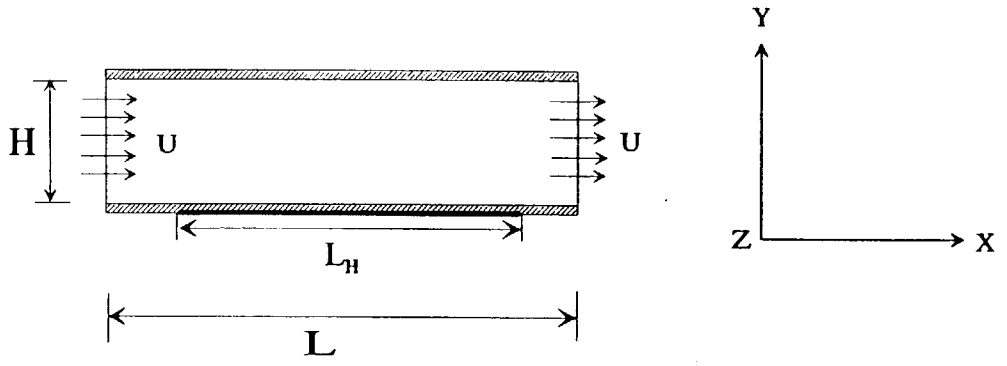

Fig. 8 2D Simulated Smooth Channel

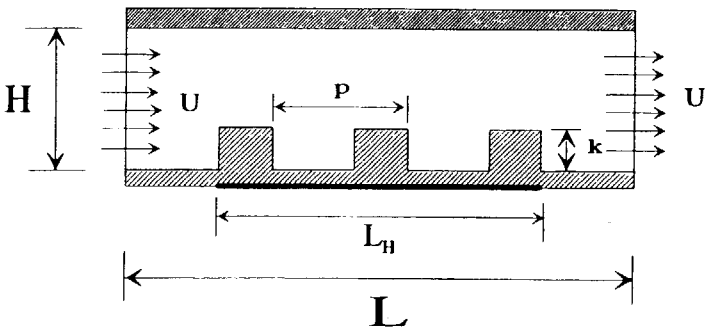

Fig. 9 2D Simulated Rib-Roughened Channel

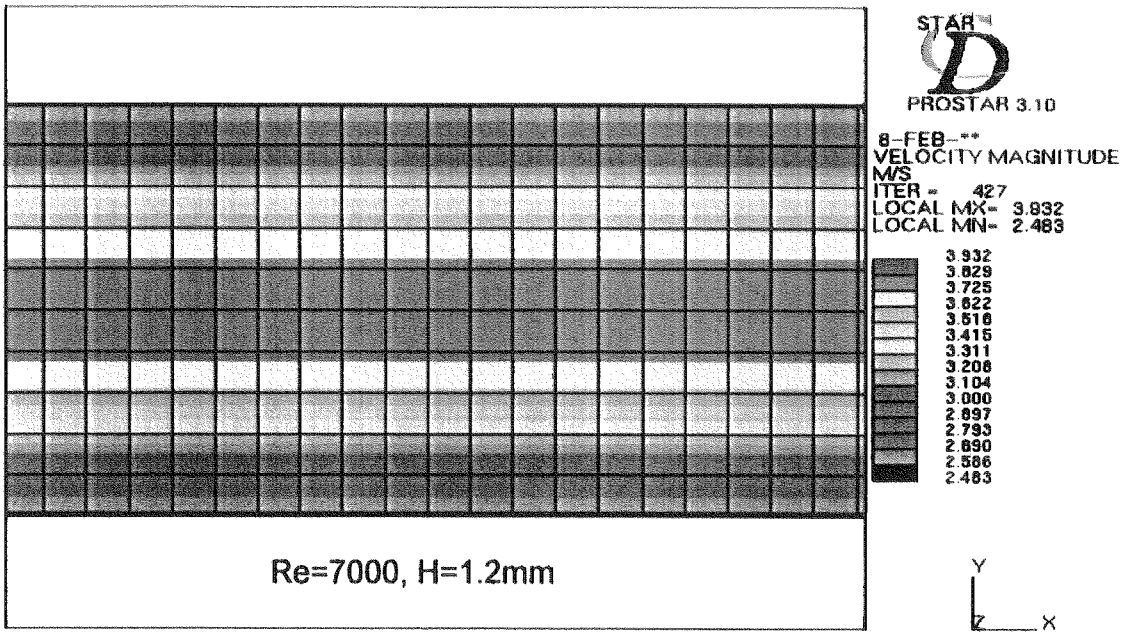

Fig. 10 Computational Grid (10 × 2000) of STD. $k-\varepsilon$ High-Re-Number Model and Velocity Magnitude(Smooth Surface)

This is a blank page.

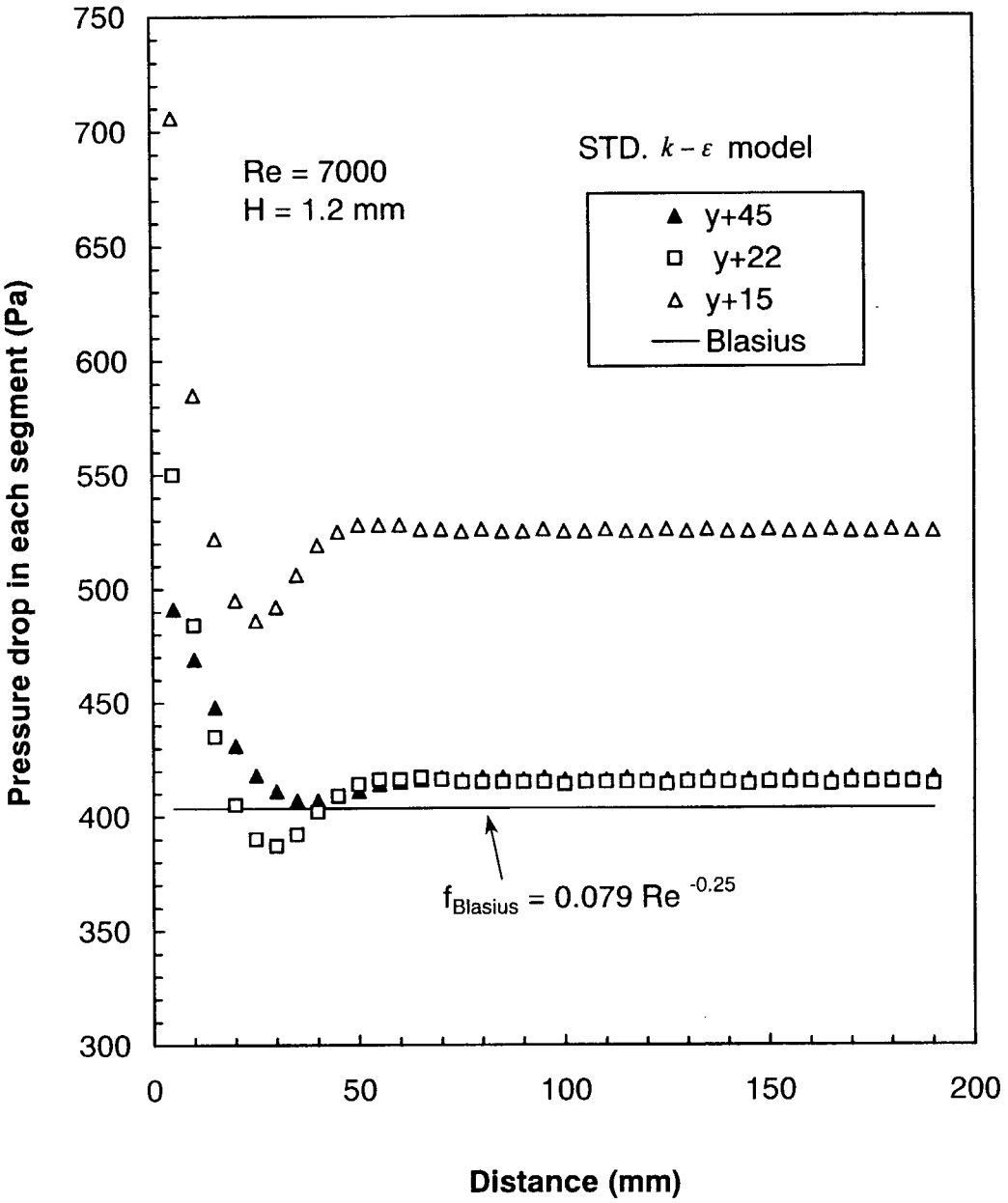

Fig. 11 Calculated Pressure Loss Distribution along Flow Direction, Re=7000

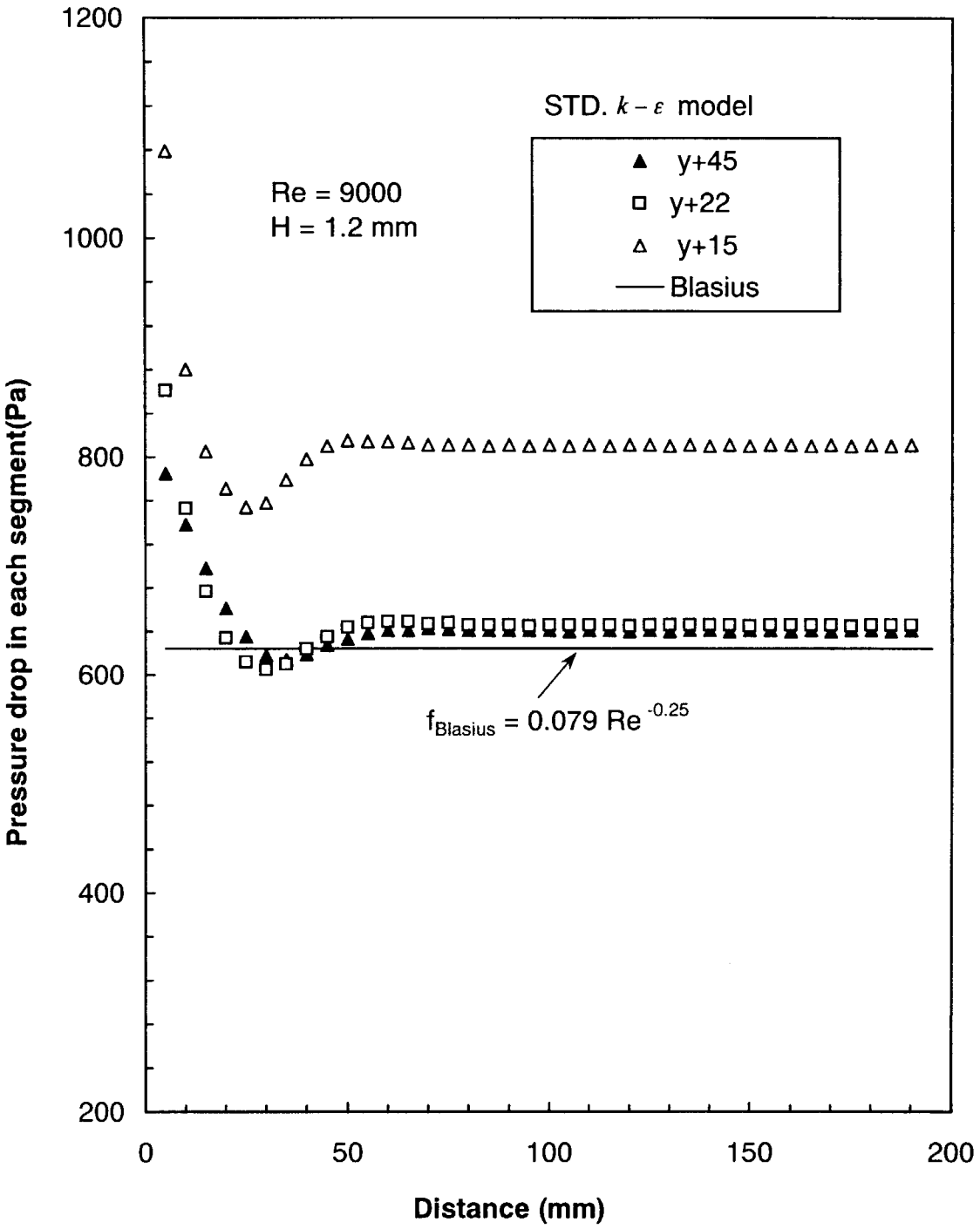

Fig. 12 Calculated Pressure Loss Distribution along Flow Direction , Re=9000

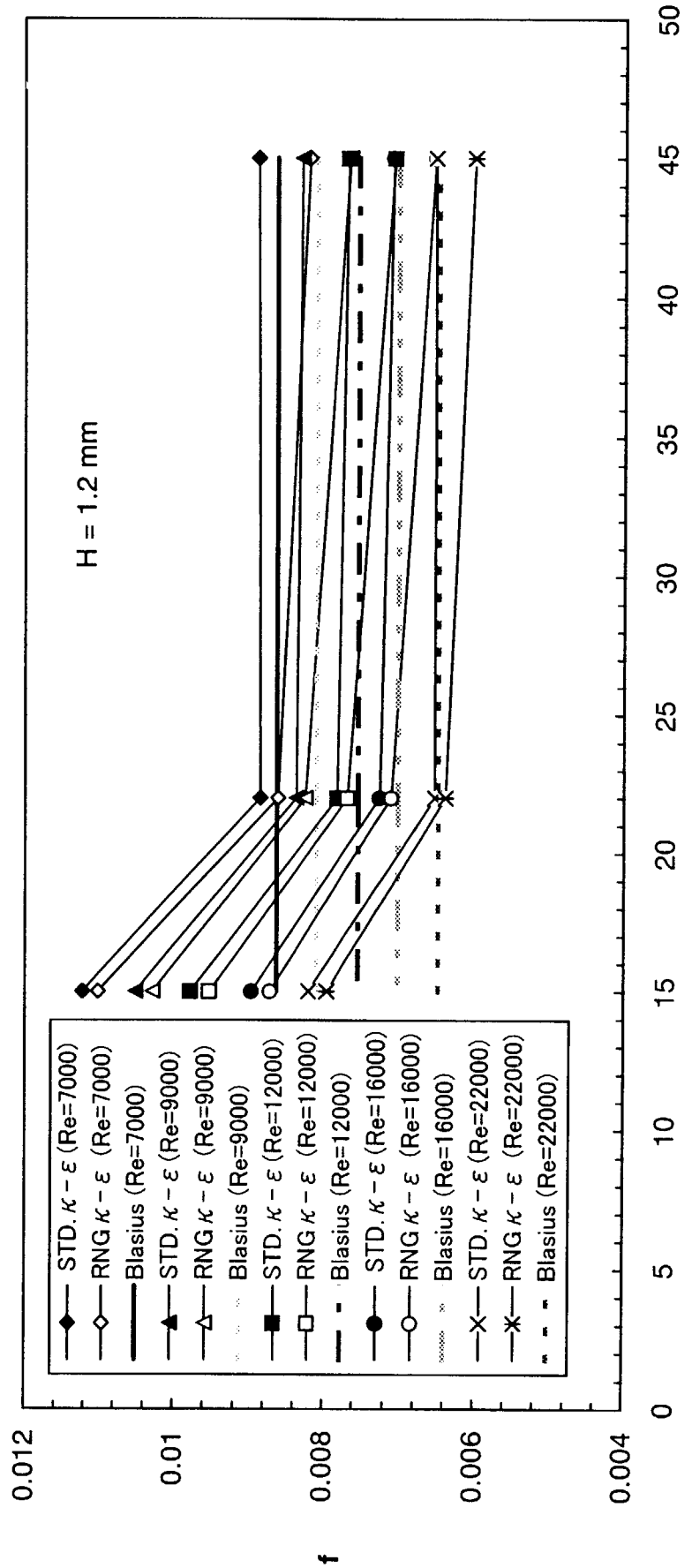

Fig. 13 Frictional Pressure Loss versus y^+

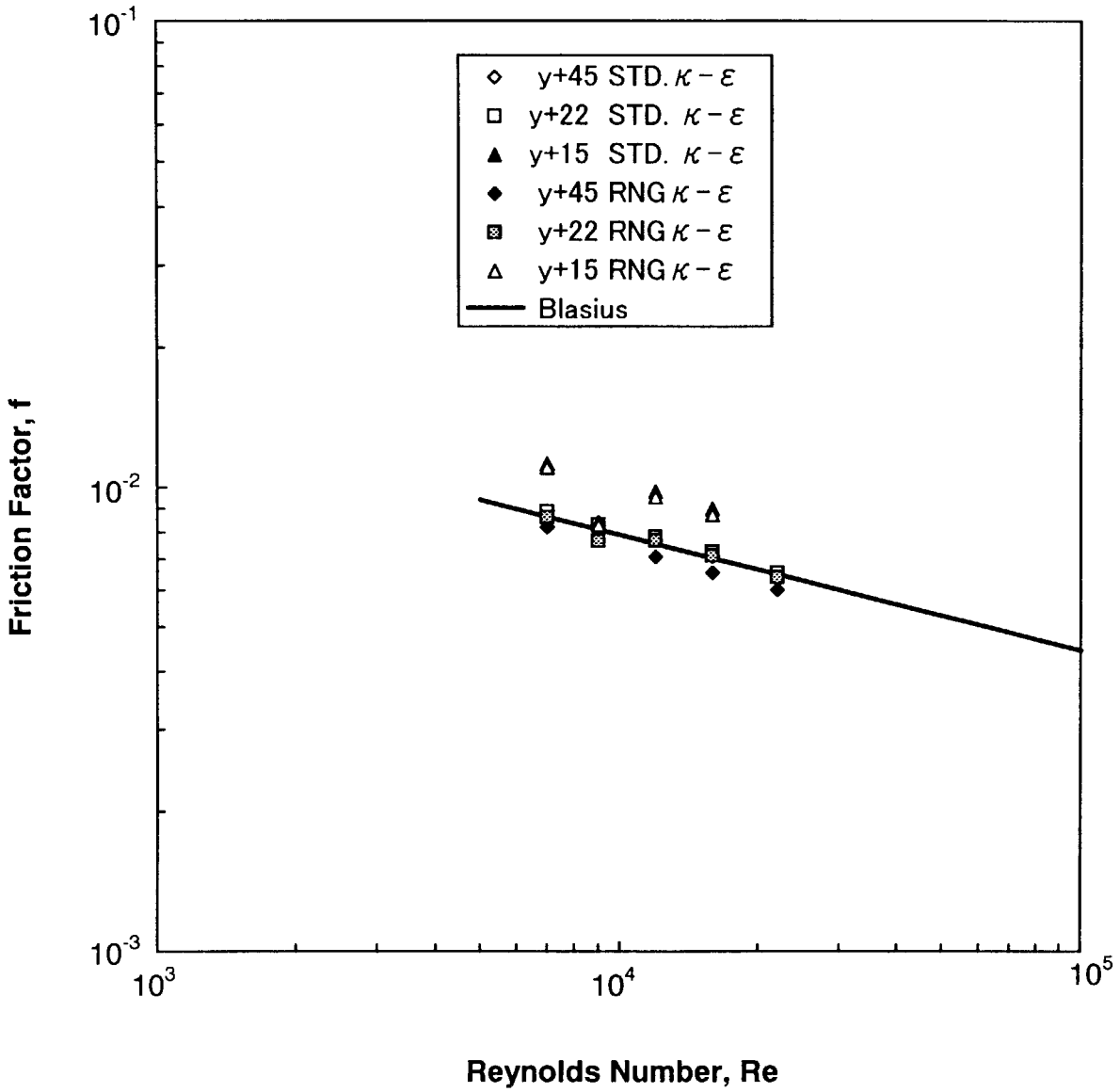

Fig. 14 Calculated Friction Factor in a Smooth Narrow Channel

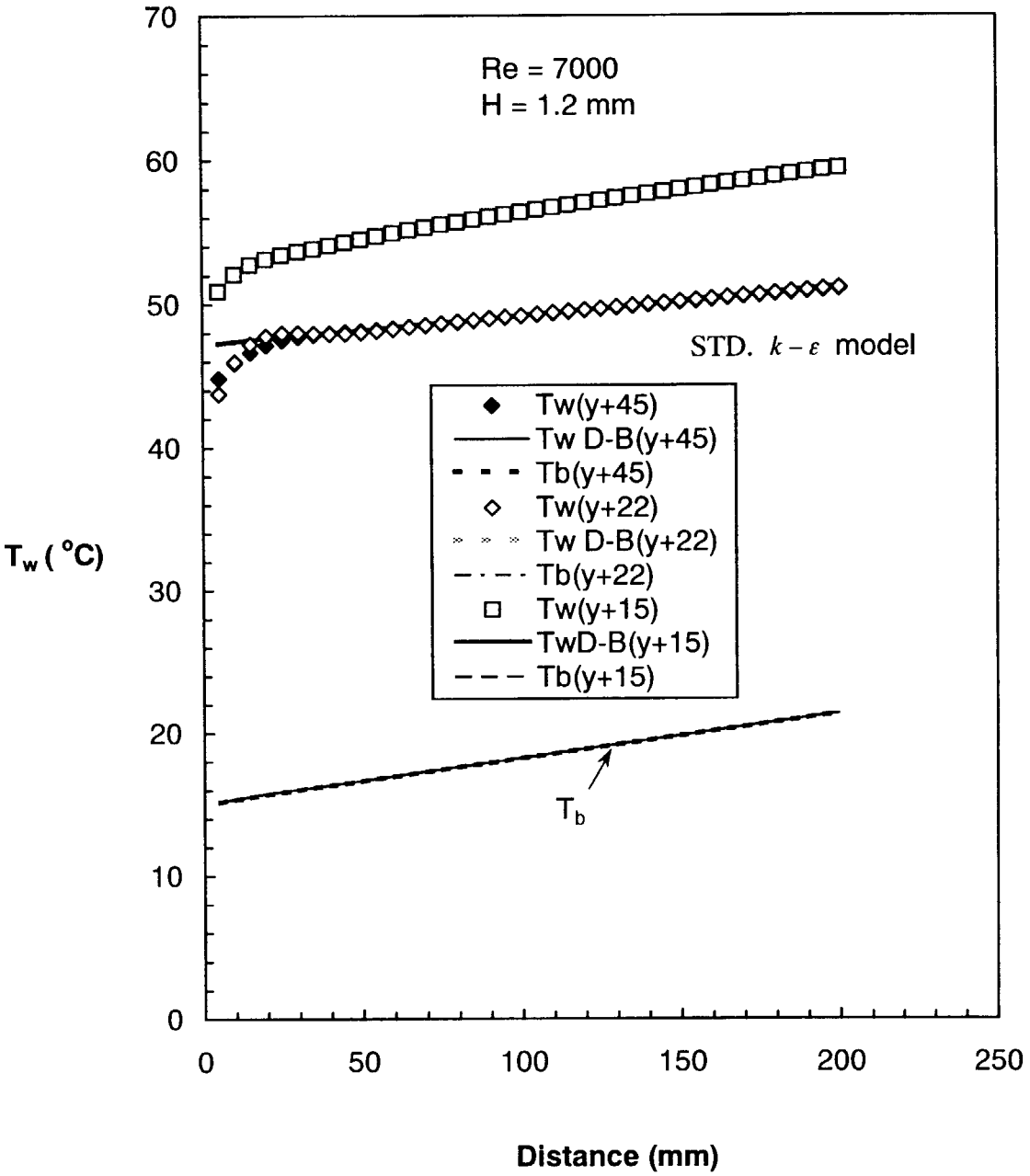

Fig. 15 Variation of T_w wrt T_b along Flow Direction

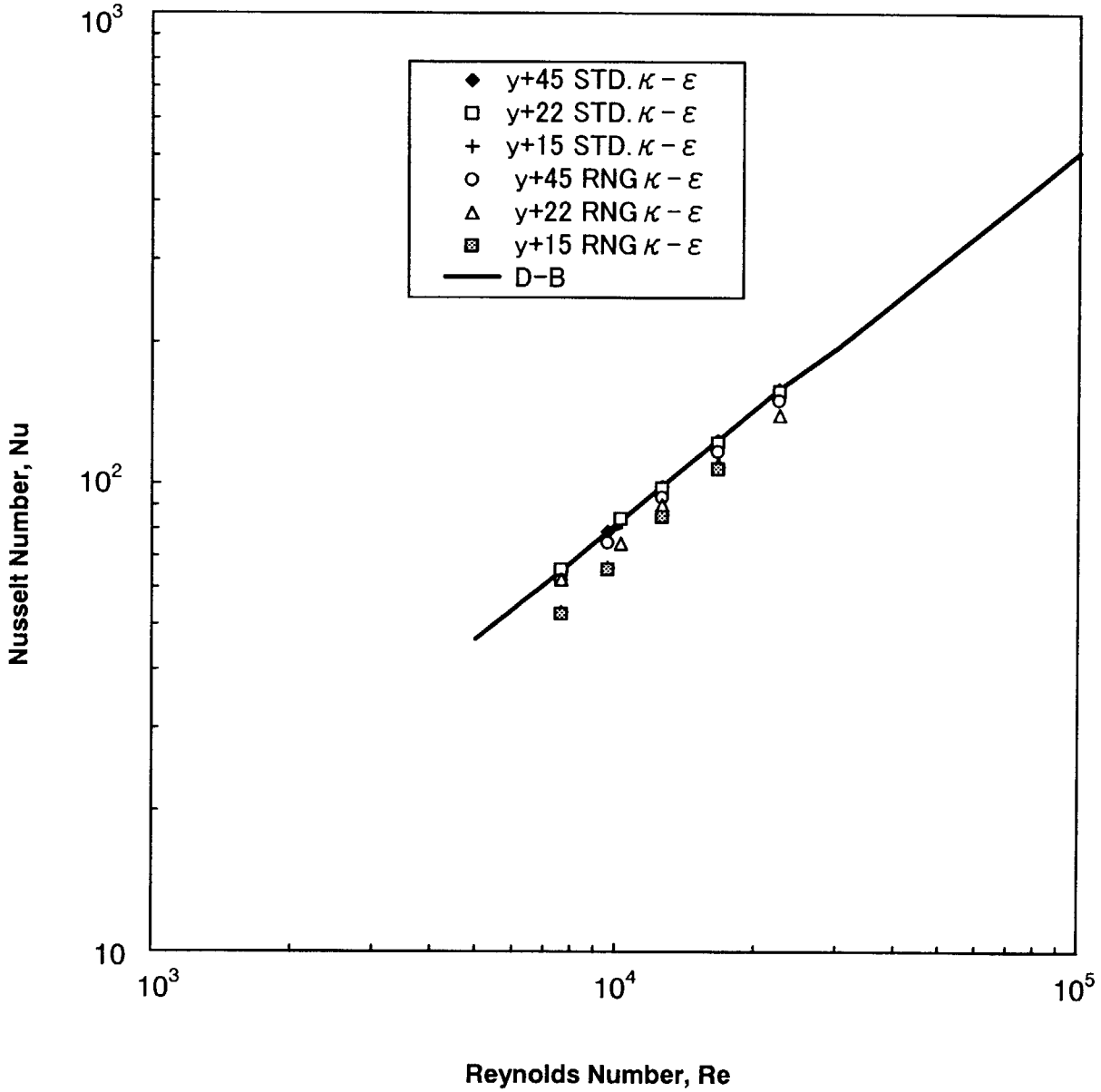

Fig. 16 Calculated Nusselt Number in a Smooth Narrow Channel

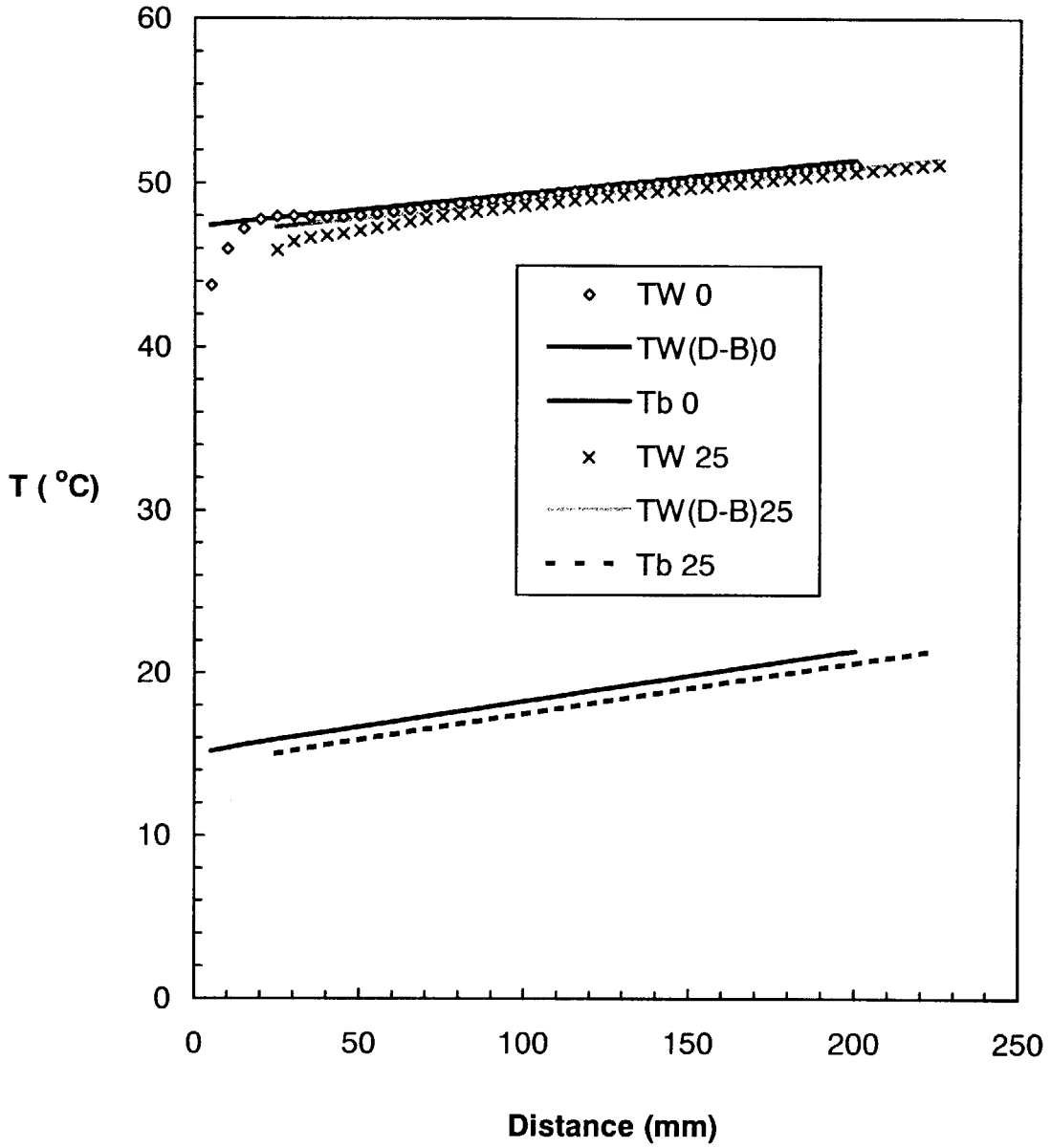

Fig. 17 Surface and Bulk Temperature Distributions along Flow Direction

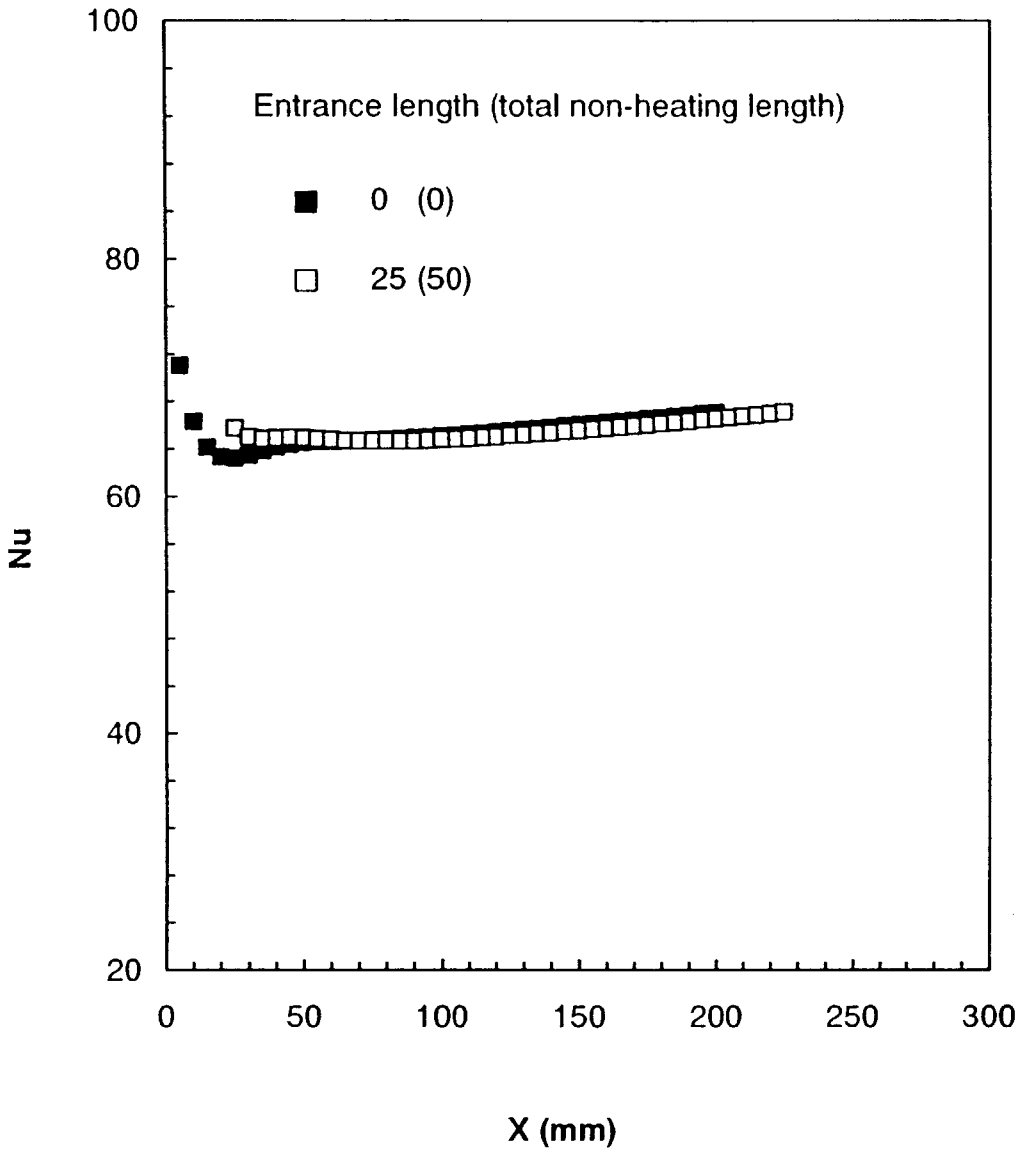

Fig. 18 Entry Length Effect on Nusselt Number

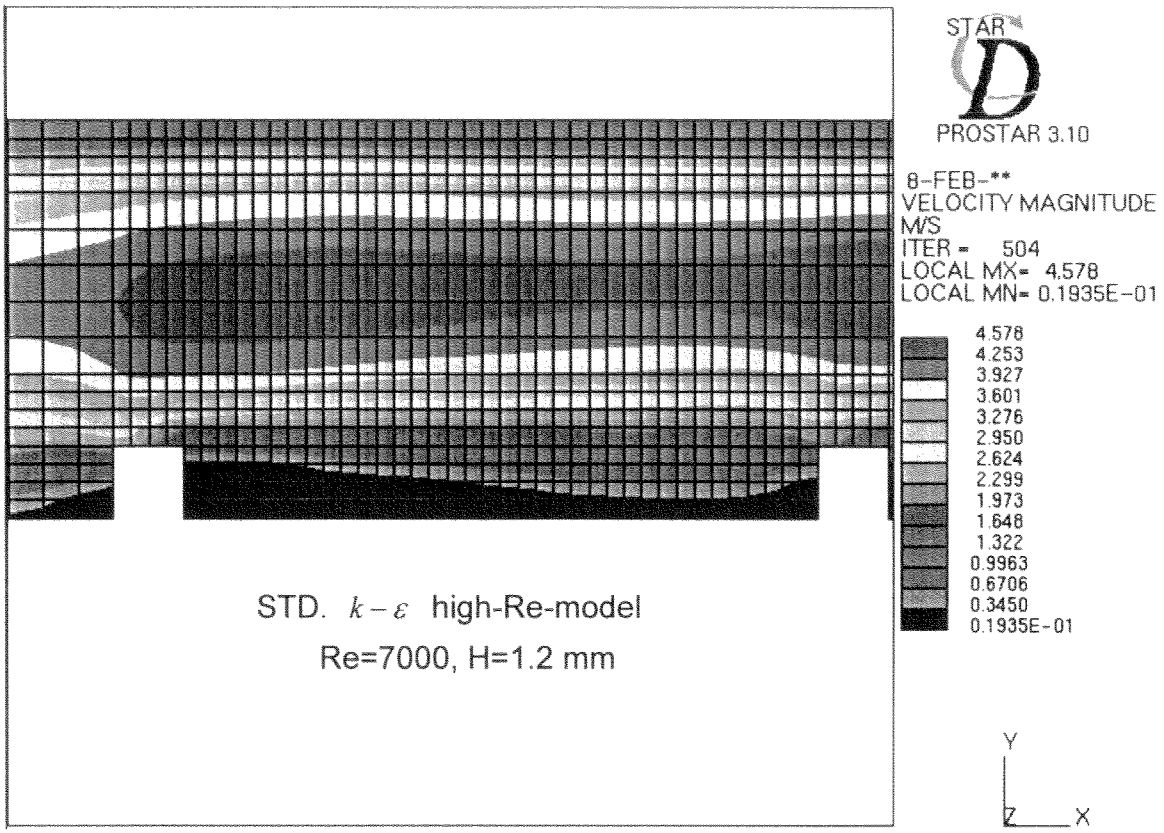

Fig. 19 Computational Grid (17 × 2000) of Rib-Roughened Geometry and Velocity Magnitude

This is a blank page.

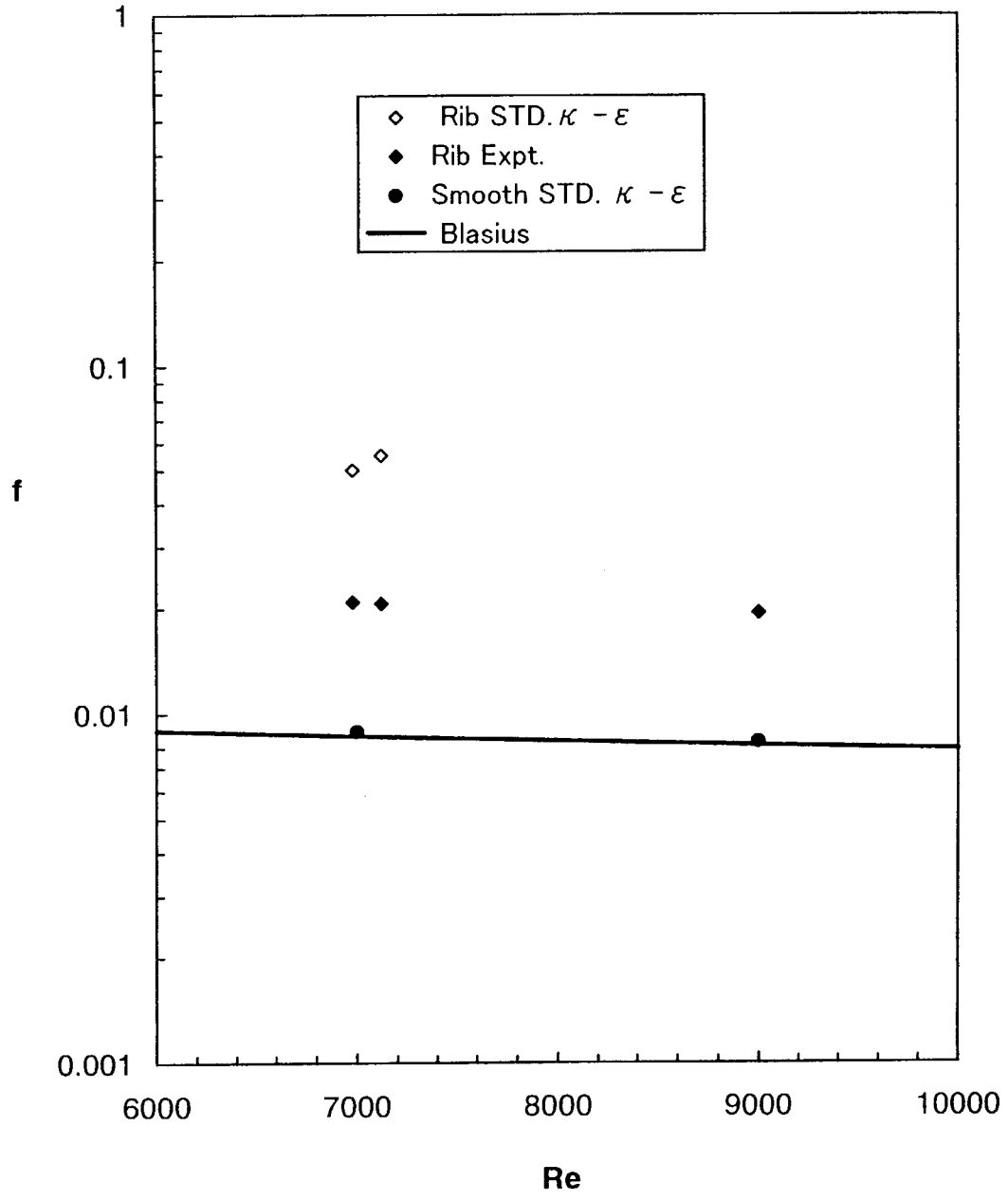

Fig. 20 Comparison of Calculated and Experimental Frictional Pressure Drops

This is a blank page.

国際単位系 (SI) と換算表

表 1　SI 基本単位および補助単位

量	名称	記号
長さ	メートル	m
質量	キログラム	kg
時間	秒	s
電流	アンペア	A
熱力学温度	ケルビン	K
物質量	モル	mol
光度	カンデラ	cd
平面角	ラジアン	rad
立体角	ステラジアン	sr

表 2　SI と併用される単位

名称	記号
分，時，日	min，h，d
度，分，秒	°，′，″
リットル	l，L
トン	t
電子ボルト	eV
原子質量単位	u

1 eV = 1.60218 × 10^{-19} J

1 u = 1.66054 × 10^{-27} kg

表 5　SI 接頭語

倍数	接頭語	記号
10^{18}	エクサ	E
10^{15}	ペタ	P
10^{12}	テラ	T
10^{9}	ギガ	G
10^{6}	メガ	M
10^{3}	キロ	k
10^{2}	ヘクト	h
10^{1}	デカ	da
10^{-1}	デシ	d
10^{-2}	センチ	c
10^{-3}	ミリ	m
10^{-6}	マイクロ	μ
10^{-9}	ナノ	n
10^{-12}	ピコ	p
10^{-15}	フェムト	f
10^{-18}	アト	a

表 3　固有の名称をもつ SI 組立単位

量	名称	記号	他の SI 単位による表現
周波数	ヘルツ	Hz	s^{-1}
力	ニュートン	N	$m \cdot kg/s^2$
圧力，応力	パスカル	Pa	N/m^2
エネルギー，仕事，熱量	ジュール	J	N·m
工率，放射束	ワット	W	J/s
電気量，電荷	クーロン	C	A·s
電位，電圧，起電力	ボルト	V	W/A
静電容量	ファラド	F	C/V
電気抵抗	オーム	Ω	V/A
コンダクタンス	ジーメンス	S	A/V
磁束	ウェーバ	Wb	V·s
磁束密度	テスラ	T	Wb/m^2
インダクタンス	ヘンリー	H	Wb/A
セルシウス温度	セルシウス度	℃	
光束	ルーメン	lm	cd·sr
照度	ルクス	lx	lm/m^2
放射能	ベクレル	Bq	s^{-1}
吸収線量	グレイ	Gy	J/kg
線量当量	シーベルト	Sv	J/kg

表 4　SI と共に暫定的に維持される単位

名称	記号
オングストローム	Å
バーン	b
バール	bar
ガル	Gal
キュリー	Ci
レントゲン	R
ラド	rad
レム	rem

1 Å = 0.1 nm = 10^{-10} m

1 b = 100 fm^2 = 10^{-28} m^2

1 bar = 0.1 MPa = 10^5 Pa

1 Gal = 1 cm/s^2 = 10^{-2} m/s^2

1 Ci = 3.7 × 10^{10} Bq

1 R = 2.58 × 10^{-4} C/kg

1 rad = 1 cGy = 10^{-2} Gy

1 rem = 1 cSv = 10^{-2} Sv

（注）

1. 表 1 ― 5 は「国際単位系」第 5 版，国際度量衡局 1985 年刊行による。ただし，1 eV および 1 u の値は CODATA の 1986 年推奨値によった。
2. 表 4 には海里，ノット，アール，ヘクタールも含まれているが日常の単位なのでここでは省略した。
3. bar は，JIS では流体の圧力を表わす場合に限り表 2 のカテゴリーに分類されている。
4. EC 閣僚理事会指令では bar，barn および「血圧の単位」mmHg を表 2 のカテゴリーに入れている。

換　算　表

力	N(=10^5 dyn)	kgf	lbf
	1	0.101972	0.224809
	9.80665	1	2.20462
	4.44822	0.453592	1

粘度　1 Pa·s(N·s/m^2) = 10 P(ポアズ)(g/(cm·s))

動粘度　1 m^2/s = 10^4 St(ストークス)(cm^2/s)

圧力	MPa(=10 bar)	kgf/cm^2	atm	mmHg(Torr)	lbf/in^2(psi)
	1	10.1972	9.86923	7.50062 × 10^3	145.038
	0.0980665	1	0.967841	735.559	14.2233
	0.101325	1.03323	1	760	14.6959
	1.33322 × 10^{-4}	1.35951 × 10^{-3}	1.31579 × 10^{-3}	1	1.93368 × 10^{-2}
	6.89476 × 10^{-3}	7.03070 × 10^{-2}	6.80460 × 10^{-2}	51.7149	1

エネルギー・仕事・熱量	J(=10^7 erg)	kgf·m	kW·h	cal(計量法)	Btu	ft·lbf	eV
	1	0.101972	2.77778 × 10^{-7}	0.238889	9.47813 × 10^{-4}	0.737562	6.24150 × 10^{18}
	9.80665	1	2.72407 × 10^{-6}	2.34270	9.29487 × 10^{-3}	7.23301	6.12082 × 10^{19}
	3.6 × 10^6	3.67098 × 10^5	1	8.59999 × 10^5	3412.13	2.65522 × 10^6	2.24694 × 10^{25}
	4.18605	0.426858	1.16279 × 10^{-6}	1	3.96759 × 10^{-3}	3.08747	2.61272 × 10^{19}
	1055.06	107.586	2.93072 × 10^{-4}	252.042	1	778.172	6.58515 × 10^{21}
	1.35582	0.138255	3.76616 × 10^{-7}	0.323890	1.28506 × 10^{-3}	1	8.46233 × 10^{18}
	1.60218 × 10^{-19}	1.63377 × 10^{-20}	4.45050 × 10^{-26}	3.82743 × 10^{-20}	1.51857 × 10^{-22}	1.18171 × 10^{-19}	1

1 cal = 4.18605 J (計量法)

= 4.184 J　(熱化学)

= 4.1855 J　(15 °C)

= 4.1868 J (国際蒸気表)

仕事率　1 PS (仏馬力)

= 75 kgf·m/s

= 735.499 W

放射能	Bq	Ci
	1	2.70270 × 10^{-11}
	3.7 × 10^{10}	1

吸収線量	Gy	rad
	1	100
	0.01	1

照射線量	C/kg	R
	1	3876
	2.58 × 10^{-4}	1

線量当量	Sv	rem
	1	100
	0.01	1

（86 年 12 月 26 日現在）

Analytical Study of Narrow Channel Flow for a Spallation Target System Design